

# Evaluating the Local Climate Zone Classification in High-Density Heterogeneous Urban Environment Using Mobile Measurement

*Yuan SHI<sup>a,\*</sup>, Kevin Ka-Lun LAU<sup>b,c,d</sup>, Chao REN<sup>a,b,c</sup>, Edward NG<sup>a,b,c</sup>*

<sup>a</sup> School of Architecture, The Chinese University of Hong Kong, Shatin, N.T., Hong Kong S.A.R., China

<sup>b</sup> The Institute of Environment, Energy and Sustainability (IEES), The Chinese University of Hong Kong, Shatin, N.T., Hong Kong S.A.R., China

<sup>c</sup> Institute Of Future Cities (IOFC), The Chinese University of Hong Kong, Shatin, N.T., Hong Kong S.A.R., China

<sup>d</sup> CUHK Jockey Club Institute of Ageing, The Chinese University of Hong Kong, Shatin, N.T., Hong Kong S.A.R., China

The corresponding author's\* email addresses: [shiyuan@cuhk.edu.hk](mailto:shiyuan@cuhk.edu.hk) (Secondary email: [shiyuan.arch.cuhk@gmail.com](mailto:shiyuan.arch.cuhk@gmail.com))

Phone: +852-39439428.

Postal addresses: Rm905, YIA Building, The Chinese University of Hong Kong, Shatin, NT, Hong Kong

## **Highlight**

- Screen-level air temperature were investigated via mobile measurements.
- Two LCZ maps of Hong Kong were evaluated using the measured air temperature data.
- Considerable temperature differences (0.5-2.5°C) were observed between LCZ classes.
- The applicability of LCZ in high-density heterogeneous urban contexts was confirmed.
- Intra-LCZ air temperature differences (up to 2 °C) in LCZs 1 to 6 were observed.

## Abstract

Urban heat island (UHI) has been identified as a threat to urban living quality in the context of climate change. As awareness of the impacts of urban expansion on local climate increases, urban planners/decision makers attempt to incorporate climatic considerations into the planning process. An increasingly-used urban climatic analysis scheme— Local Climate Zone (LCZ) classification— has been applied in Hong Kong, a high-density city with heterogeneous an urban environment. This study aims to evaluate the LCZ mapping in such a unique urban context using in-situ air temperature data. The fine-scale spatial variation of the daytime and nighttime screen-level air temperatures was investigated via mobile measurements during the summertime of 2016. The measured data were collated in Geographic Information System (GIS) based on the current LCZ maps. Statistically significant air temperature differences were observed between most LCZ classes, which confirm the veracity of LCZ in high-density heterogeneous urban contexts. Higher uncertainties in the site-averaged air temperature and considerable intra-LCZ air temperature differences in LCZs 1 to 6 were observed. It indicates that the current LCZ procedures of Hong Kong can be further refined for a better understanding of the climatic heterogeneity in densely built urban areas.

**Keywords:** urban heat island; Local Climate Zone (LCZ); World Urban Database and Access Portal Tools (WUDAPT); mobile measurement; high-density city; Hong Kong

## 1. Introduction

1  
2  
3 Extreme weather events, such as heat waves, are becoming more frequent and intense amid  
4  
5 climate change (IPCC 2014). Such trend will have a tremendous effect on health  
6  
7 (McMichael, Woodruff, and Hales 2006, WHO 2003), particularly in highly urbanized and  
8  
9 sprawling cities (Stone, Hess, and Frumkin 2010). Furthermore, due to the Urban Heat Island  
10  
11 (UHI) phenomenon in highly urbanized areas, the impact of heat wave could be further  
12  
13 intensified (Tan et al. 2010). As one of the densest and most populated cities in the world,  
14  
15 Hong Kong is particularly susceptible to severe heat-related health consequences (Chan et al.  
16  
17 2012). Traditionally, the UHI intensity is described as the air temperature difference between  
18  
19 the urban area and its surrounding rural areas (Rizwan, Dennis, and Liu 2008). However,  
20  
21 under a heterogeneous urban context, this definition is inadequate to depict the intra-urban  
22  
23 differences in air temperature between different districts in a large city (Chen et al. 2012,  
24  
25 Stewart and Oke 2012, Oke 2004, Lowry 1977).  
26  
27  
28  
29  
30  
31

32  
33 Urban form is closely related to the urban climate (Eliasson 1990). The forms of urban  
34  
35 planning and development are influential to the local climatic conditions (Grimmond 2007)  
36  
37 because the urban environment alters the wind flow, radiation balance, water and heat  
38  
39 balances (Landsberg 1981). Urban expansion without appropriate planning control leads to  
40  
41 substantial environmental degradation (Betanzo 2007). As awareness of the impacts of urban  
42  
43 expansion on local climate grows, urban planners and decision makers have started to  
44  
45 incorporate the climatic consideration into the planning process (Eliasson 2000).  
46  
47  
48  
49

50  
51 To provide a better spatial understanding of local climate and help planners improve the  
52  
53 urban form based on the climatic consideration, several classification schemes have been  
54  
55 developed. They are the Urban Zones of Energy partitioning (UZE) (Loridan and Grimmond  
56  
57 2012, Loridan et al. 2013), Urban Climatic Map (UCMap) system (Ren, Ng, and Katzschner  
58  
59  
60  
61  
62  
63  
64  
65

1 2011), Urban Climate Zone (UCZ) scheme (Oke 2004, 2006) and Local Climate Zone (LCZ)  
2 scheme (Stewart and Oke 2012). The common theme of these different schemes is that all of  
3  
4 them are established according to the information from urban indicators. These urban  
5  
6 indicators include but are not limited to the land use/land cover (LU/LC) pattern, topographic,  
7  
8 surface geometry and climatic spatial information. Based on this information, the above  
9  
10 mentioned zoning systems/schemes can depict the effects of the spatially varied urban  
11  
12 environment on local climate modifications. Urban form and function classification are  
13  
14 standardized in the LCZ scheme, making it possible to provide a more detailed spatial  
15  
16 understanding of the variability of intra-urban air temperature, rather than a simple  
17  
18 description of urban-rural difference (Stewart and Oke 2012). The LCZ scheme was  
19  
20 developed and serves as a global standard for depicting different urban morphologies  
21  
22 (Stewart and Oke 2009). The scheme features 17 types of LCZ classes, including ten built  
23  
24 types (LCZ 1 to LCZ 10), and seven land cover types (LCZ A to LCZ G). A full list of LCZ  
25  
26 classes is shown in  
27  
28  
29  
30  
31  
32

33  
34  
35 *Table 1.*  
36

37  
38 The properties of each LCZ class can be differentiated by metadata of urban land use and  
39  
40 morphological factors (Stewart and Oke 2012). LCZs generated following the highly  
41  
42 standardized scheme can help examine the UHI phenomenon in different cities. The  
43  
44 advantage of the LCZ scheme over tradition land-use classification methods is that it also  
45  
46 takes urban morphological details into consideration, which advances urban climatic  
47  
48 research. Therefore, LCZ has been used in many different cities around the world for  
49  
50 mapping (Bechtel et al. 2015). Moreover, to generate an internationally standardized LCZ  
51  
52 classification database, a new project —World Urban Database and Access Portal Tools  
53  
54 (WUDAPT)— was initiated in 2012 (Mills et al. 2015). It aims to develop LCZ maps for  
55  
56 cities where detailed urban morphological data are not available using open-source remote  
57  
58  
59  
60  
61  
62  
63  
64  
65

1 sensing data. The performance of WUDAPT data in urban climatic analysis and the  
2 subsequent urban planning processes, in terms of accuracy and relevance, therefore requires  
3 comprehensive assessment (Stewart, Oke, and Krayenhoff 2014).  
4  
5  
6

7 In Hong Kong, a prior study has classified 17 weather stations in the weather monitoring  
8 network of the Hong Kong Observatory (HKO) into LCZ scheme for UHI quantification (Siu  
9 and Hart 2012). After that, to develop climate-adapted urban planning and design strategies  
10 for the local practice, another study has further developed an LCZ classification map (with a  
11 spatial resolution of 300m) for Hong Kong—a high-density large city with a highly  
12 heterogeneous urban environment (Zheng et al. 2017). The study’s mapping method was  
13 GIS-based and it was possible because sufficient and detailed data of urban indicators are  
14 available in Hong Kong from the local planning department (PlanD). A set of LCZ maps with  
15 a finer spatial resolution of 100m (a WUDAPT level 0 product) was also developed using the  
16 WUDAPT method to align the LCZ map of Hong Kong with worldwide research (Ren et al.  
17 2016). The mapping accuracy of both of the above studies was evaluated in the study of  
18 Wang et al. (2017). The spatial pattern of the resultant LCZ maps showed a high consistency  
19 with the previous UCMaps system of Hong Kong. However, intra-LCZ site variations of  
20 urban indicators were also detected in the built-up LCZ classes (particularly LCZ1-6, see  
21 Table 1 and Figure 1) of the resultant maps. It confirms the necessity of validation using  
22 measured air temperature data. The above also indicates the potential of further optimization  
23 of the LCZ classification procedure in a high-density urban scenario.  
24  
25  
26  
27  
28  
29  
30  
31  
32  
33  
34  
35  
36  
37  
38  
39  
40  
41  
42  
43  
44  
45  
46  
47  
48

49 Mobile measurement using moving vehicles has been regarded a cost-effective method to  
50 investigate intra-urban environmental variability (Peters, Van Poppel, and Theunis 2012,  
51 Peppler 1929). It fills the monitoring gaps of the sparsely distributed fixed monitoring  
52 locations by providing more spatial information. This method has been increasingly adopted  
53  
54  
55  
56  
57  
58  
59  
60  
61  
62  
63  
64  
65

1 and continuously improved in UHI investigation (Liu et al. 2016, Tsin et al. 2016, Stewart  
2 2011). Air temperature data acquired by the mobile measurement method have been used for  
3  
4 many different study purposes. For example, they were employed to characterize the urban-  
5 rural air temperature difference (Hedquist and Brazel 2006, Unger, Sümeghy, and Zoboki  
6 2001), correlate urban air temperature with remotely sensed land surface temperature (LST),  
7 understand the relationship between the microclimate condition and urban geometry  
8  
9 (Blankenstein and Kuttler 2004, Tsin et al. 2016), and evaluate the cooling effects of urban  
10 greenery (Lu et al. 2012). In Hong Kong, a few prior air temperature studies have made use  
11 of mobile measurement in both urban built-up and rural areas (Nichol et al. 2009, Zheng et al.  
12 2015). The success of these studies confirms the feasibility of monitoring microscale spatial  
13 variation of air temperature and the potential of validating further studies using the mobile  
14 measurement method.  
15  
16  
17  
18  
19  
20  
21  
22  
23  
24  
25  
26  
27  
28

29 Recently, the mobile measurement method has gained popularity and success in LCZ  
30 classification and spatialization studies (Szymanowski and Kryza 2009, Alexander and Mills  
31 2014). Observation-based LCZ studies are normally based on urban meteorological networks  
32 (Skarbit et al. 2017, Lehnert et al. 2015, Unger et al. 2015). The fixed monitoring networks  
33 work well in mid-density cities in Europe and North America that are more uniformly  
34 developed with discreet patterns of land use and urban form. However, the geographic setting  
35 and urban contexts of many densely populated large cities (especially in Asia) are more  
36 heterogeneous and complex. Such geographic complexity with mixed forms results in large  
37 air temperature variations between and within different LCZ classes of the city at a relatively  
38 smaller spatial scale. Such spatial variations cannot be effectively investigated by fixed  
39 monitoring networks alone. To evaluate LCZ classification/mapping, a comprehensive  
40 understanding of the spatial variation of air temperature needs to be acquired. The spatial  
41 advantages of mobile measurement make it ideal for investigating the relationship between  
42  
43  
44  
45  
46  
47  
48  
49  
50  
51  
52  
53  
54  
55  
56  
57  
58  
59  
60  
61  
62  
63  
64  
65

1 the urban built-up surface and the near-surface air temperature. Therefore, the mobile  
2 measurement method has been further applied in the evaluation of the LCZ-based UHI  
3 assessment (Leconte et al. 2015, Kotharkar and Bagade 2018).  
4  
5  
6

7 The mobile platform is particularly useful in the investigation of the screen-level  
8 environmental variation in Hong Kong because of its unique urban environment (Shi, Lau,  
9 and Ng 2016). Previous mobile measurement case cities in North America and European  
10 have been done in a relatively simple urban context that shows more uniformly discreet  
11 patterns of land use and urban form. However, downtown areas in Hong Kong are high-  
12 density high-rise and their urban context is highly inhomogeneous in terms of urban  
13 morphology and mixed land use at local scales. Its extreme heterogeneity and high-density  
14 high-rise environment can possibly lead to a large difference between the ambient air  
15 temperature measured by the fixed monitoring locations in the network of HKO weather  
16 stations and the screen-level air temperature via mobile measurement. The consideration is  
17 particularly important in the street canyons of the high-density downtown area. Under such  
18 circumstance, the screen-level air temperature measured using the mobile platform has a  
19 better potential to reflect the actual situation of people's outdoor heat exposure and is more  
20 informative to UHI investigation and health impact assessments.  
21  
22  
23  
24  
25  
26  
27  
28  
29  
30  
31  
32  
33  
34  
35  
36  
37  
38  
39  
40  
41

42 This study uses mobile measurement to evaluate the performance of the current LCZ  
43 mappings (results from both the GIS-based method and WUDAPT method) of Hong Kong in  
44 determining the spatial variation of UHI and informing urban climatic studies. In the present  
45 study, air temperature differences between LCZ classifications and the intra-LCZ temperature  
46 variability were extracted from the mobile measurement data set. Further assessments were  
47 then conducted for the current LCZ mapping schemes of Hong Kong. The study results  
48 indicate that LCZ measurement and mapping systems in Hong Kong could be optimized  
49 through some improvement strategies.  
50  
51  
52  
53  
54  
55  
56  
57  
58  
59  
60  
61



## 2. Materials, Methods, and Study Area

### 2.1. The Geographic and Urban Context of Hong Kong

Hong Kong is a subtropical city located on the southeast coast of China (22° 150' N, 114° 100' E. Figure 3 shows the location). Its subtropical maritime weather features hot humid summer with occasional showers and thunderstorms and warm winter. Hong Kong has abundant natural green resources, a hilly topography, coastal landscapes and diverse geological features in its countryside. More than 70% of land (measuring approximately 1100 km<sup>2</sup>) is vegetated mountainous areas and country parks (Taylor 1986). Only less than a quarter of the land resources in regions with a relatively flat topography and at a lower elevation are used for urban development (PlanD 2015). The complex urban morphology due to mixed land use is primarily due to the geographical constraints and urban development oriented to major transportation corridors. Urban centres were developed along transportation nodes and are self-sustained in nature. As such, land utilization is characterized by the diverse nature. In addition, the large population requires a high-density and high-rise mode of development. Both natural and artificial land cover types in Hong Kong are very diverse. The mixture of different landscapes shapes the unique urban context of Hong Kong (Figure 1-a, b).

### 2.2. Current LCZ Classification and Spatial Map of Hong Kong

#### 2.2.1. GIS-based Mapping

As mentioned, a GIS-based LCZ classification has been developed for high-density Hong Kong. The criteria are described as follows (Zheng et al. 2017):

First, built-up classes and land cover classes were separated by reclassifying the land use data of Hong Kong. Then, for built-up classes (LCZ 1 to LCZ 10), LCZ 10 was identified based

1 on the industrial land use type, and LCZ 1 to LCZ 9 were quantitatively differentiated based  
2 on three building morphological factors - building surface fraction ( $\lambda_b$ , [0-1]), building height  
3 ( $Z_h$ , unit: m), and sky view factor ( $\Psi_{svf}$ , [0-1]). Stewart and Oke (2012) proposed a set of  
4 standard values of geometric and surface cover properties for LCZs. Among them, four  
5 parameters are about the urban surface roughness - canyon aspect ratio (H/W) and  $\lambda_b$ ,  $Z_h$ ,  
6 terrain roughness class. Instead of including all morphological factors, only three key factors  
7 were used as parameters for the LCZ classification in this study. For example,  $\Psi_{svf}$  is  
8 essentially correlated with H/W (Oke 1981). Moreover, it has been tested that the  $\Psi_{svf}$  is a  
9 very good indicator of intra-urban air temperature differentials in the high-rise high-density  
10 urban areas of Hong Kong (Chen et al. 2012). Therefore,  $\Psi_{svf}$  was used. The criteria for  
11 terrain roughness class were set up based on the Davenport et al. (2000)'s classification,  
12 which is not suitable for depicting high-density urban morphology [most of the built-up areas  
13 can only be classified into Class 8 "Skimming: City center ( $z_0 \geq 2$ )"] (Ng et al. 2011).  
14 Therefore, we used  $Z_h$  for the classification. All building morphological factors were  
15 calculated and mapped at a spatial resolution of 100m.  
16  
17  
18  
19  
20  
21  
22  
23  
24  
25  
26  
27  
28  
29  
30  
31  
32  
33  
34  
35  
36  
37

38 Table 1 shows the quantitative classification scheme of the built-up classes. For rural areas, a  
39 total of seven land cover classes (LCZ A - G) were further classified based on the land use  
40 type. The finalized LCZ map of Hong Kong is shown in Figure 1-c. It has been found that  
41 LCZ classification results are often sensitive to the spatial scale of the LCZ site or mapping  
42 resolution, especially in Asia cities due to their unique urban contexts and heterogeneous  
43 urban environment (Kotharkar and Bagade 2017). Therefore, it is necessary to determine an  
44 appropriate spatial size of LCZ site before LCZ mapping. The map was produced at a spatial  
45 resolution of 300m— the optimal spatial size of the LCZ site of Hong Kong according to Lau,  
46 Ren, et al. (2015). It should be noted that LCZ 7 and LCZ 8 were not detected by the GIS-  
47  
48  
49  
50  
51  
52  
53  
54  
55  
56  
57  
58  
59  
60  
61  
62  
63  
64  
65

based method, probably due to the extremely small areal proportion. The areas of LCZ 7 and LCZ 8 detected by WUDAPT method were quite small as well (1.22 km<sup>2</sup> and 1.08 km<sup>2</sup>).

**Table 1.** Criteria for GIS-based classification of LCZs in Hong Kong. Values for LCZs 1 to 9 are from Stewart and Oke (2012). Criteria for LCZs 10 to G are adapted from local urban planning datasets of Hong Kong (Wang et al. 2017).

LCZ Classes	Criteria of Classification
LCZ 1-Compact High-rise	$0.4 < \lambda_b < 0.6$ and $Z_h > 25$
LCZ 2-Compact Mid-rise	$0.4 < \lambda_b < 0.7$ and $10 < Z_h < 25$
LCZ 3-Compact Low-rise	$0.4 < \lambda_b < 0.7$ and $3 < Z_h < 10$
LCZ 4-Open High-rise	$0.2 < \lambda_b < 0.4$ and $Z_h > 25$
LCZ 5-Open Mid-rise	$0.2 < \lambda_b < 0.4$ and $10 < Z_h < 25$
LCZ 6-Open Low-rise	$0.2 < \lambda_b < 0.4$ , $3 < Z_h < 10$
LCZ 7-Lightweight Low-rise	$0.6 < \lambda_b < 0.9$ , $2 < Z_h < 4$ , $0.2 < \Psi_{svf} < 0.5$
LCZ 8-Large Low-rise	$0.3 < \lambda_b < 0.5$ , $3 < Z_h < 10$ , $\Psi_{svf} > 0.7$
LCZ 9-Sparsely Built	$0.1 < \lambda_b < 0.2$ , $3 < Z_h < 10$ , $\Psi_{svf} > 0.8$
LCZ 10-Heavy Industry	LU/LC = Industrial Land
LCZ A-Dense Trees LCZ B-Scattered Trees	LU/LC = Woodland (LCZ A/B were combined due to the lack of information on wood species.)
LCZ C-Bush, Scrub	LU/LC = Shrub Land
LCZ D-Low Plants	LU/LC = Agricultural Land
LCZ E-Bare Rock or Paved	LU/LC = Roads, Railway, Airport, Quarries, Rocky Shore
LCZ F-Bare Soil or Sand	LU/LC = Badland, Vacant Development Land/Construction in Progress
LCZ G-Water	LU/LC = Reservoirs, Streams and Nullahs

### 2.2.2. WUDAPT Mapping

Unlike the GIS-based LCZ classification method, the WUDAPT level 0 mapping product follows a set of standard procedures for data collection and processing (See et al. 2015).

Following the procedure described by Bechtel et al. (2015), Landsat 8 satellite images from the United States Geological Survey (USGS) were chosen as the data source for the WUDAPT mapping of Hong Kong. Using the method of visual interpretation, training samples were selected to represent each LCZ class with the help from urban planning experts familiar with the urban context of Hong Kong. WUDAPT identifies LCZ classes by random forest algorithm. This machine learning algorithm builds a decision tree based on the spectral

features/patterns contained by the training samples. As a result, the WUDAPT level 0 map at a finer spatial resolution of 100m was produced (Figure 1-d).

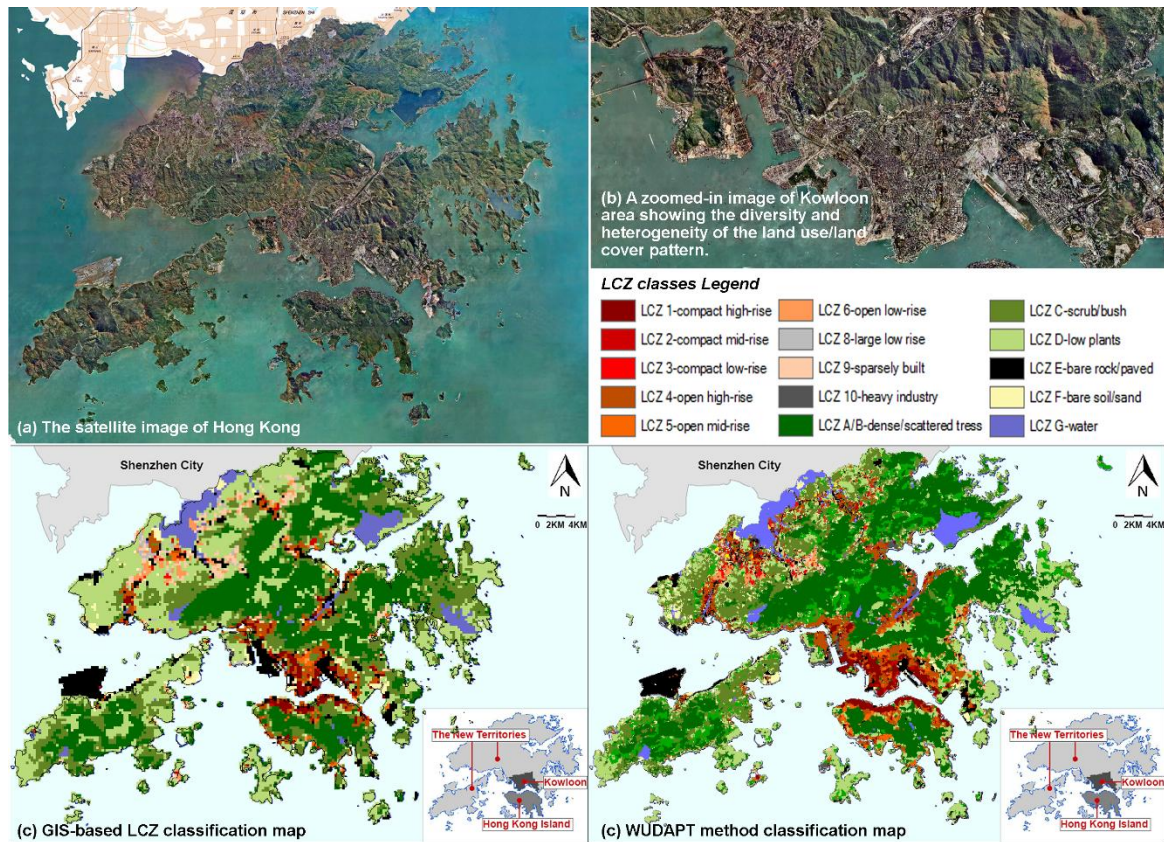


**Figure 1.** The satellite images - (a) and (b), current GIS-based LCZ map (c) (Zheng et al. 2017), and WUDAPT map (d) (Wang et al. 2017) of Hong Kong.

### 2.3. Measuring Screen-level Air Temperature Using Mobile Platform

In this present study, mobile measurement campaigns were conducted during the summertime of the year of 2016. The spatial distribution of both the daytime and nighttime screen-level air temperature was investigated. The measured air temperature data were collated with the current LCZ classifications/WUDAPT maps of Hong Kong.

#### 2.3.1. Mobile Measurement Platform

A light-colored Toyota bB mini MPV vehicle installed with microclimate sensors was used as the mobile platform for all measurement campaigns in this present study (Figure 2 and

1  
2  
3  
4  
5  
6  
7  
8  
9  
10  
11  
12  
13  
14  
15  
16  
17  
18  
19  
20  
21  
22  
23  
24  
25  
26  
27  
28  
29  
30  
31  
32  
33  
34  
35  
36  
37  
38  
39  
40  
41  
42  
43  
44  
45  
46  
47  
48  
49  
50  
51  
52  
53  
54  
55  
56  
57  
58  
59  
60  
61  
62  
63  
64  
65

Table 2). The air temperature ( $T_a$ , °C) and relative humidity ( $RH$ , %) were measured and logged at a time interval of one second using TESTO™ 480 Thermometers with the sensor - Humidity and Temperature Probe Ø 12 mm. The geographical position of each measurement was simultaneously recorded with a Garmin™ GPS Map 62s Handheld Navigator. A wide-angle video camera was installed at the front windshield of the vehicle to continuously record the surroundings during the entire process of each measurement campaign, providing a reference for the identification of any other influential factors of the temperature and humidity measurements. All microclimate sensors used in the mobile measurement were calibrated before the mobile measurement campaigns. They were solely used for the mobile measurement in this study and were maintained appropriately by professional technicians to ensure reliability.

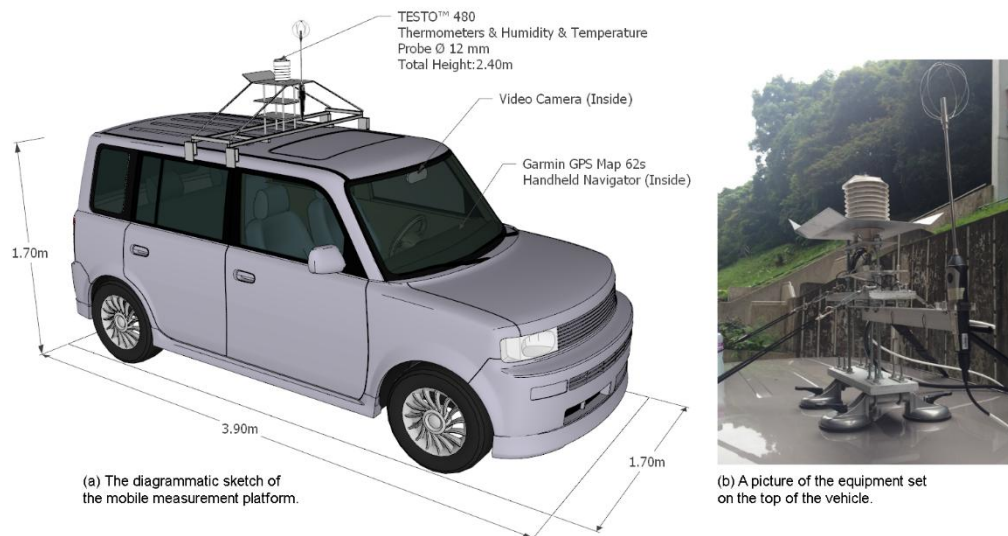


**Figure 2.** *The mobile measurement platform.*

**Table 2.** Summary of measurement equipment installed on the mobile measurement platform.

<i>Installed Instruments</i>	<i>Measured Parameter</i>	<i>Measuring Interval</i>	<i>Accuracy of the Instruments</i>	<i>Data Category</i>
TESTO™ 480 Thermometers & Humidity and Temperature Probe Ø 12 mm	Air temperature ( $T_a$ , °C) & Relative humidity ( $RH$ , %)	1s (1Hz frequency-measurement)	$T_a$ : $\pm 0.3$ °C (-20 to +70 °C) $RH$ : $\pm 2$ % (2 to 98 %)	Meteorological data
Garmin™ GPS Map 62s Handheld Navigator	Latitude, Longitude, Altitude	1s (1Hz frequency-measurement)	Error within $\pm 3.7$ m (12Feet)	GPS data
Video Camera	Driving video records	30FPS	N.A.	Referential video records

### 2.3.2. Protocols of the Mobile Measurement Campaigns

Two measurement routes with a total length of approximately 90km were designed to cover a broad range of LCZ sites (Figure 3). The length of route-1 was 35km, and route-2 was 55km. Route-1 covered more built-up areas, while route-2 passed through more land cover classes. The routes were also designed based on the areal proportion of different LCZ classes. As a result, the composition of the route length in different LCZ classes is proportional to the areal proportion of different classes in the LCZ map mentioned above (Figure 4). Most of the built-up urban areas of Hong Kong are in regions with a relatively flat topography and at a lower elevation (The mean elevation is approximately 24m. Most of the built-up areas is below the elevation of 60m. See Figure 3). Therefore, hilly areas were also avoided during the design of the mobile measurement routes. The elevation of most parts of the two routes approximately ranged from 10m to 60m without steep slopes. Moreover, most parts of the routes were far from the coastline with a distance of larger than 1000m. The few road segments closer to the coastline were approximately 100m to 200m from it. A couple of pilot tests were conducted before the mobile measurement campaigns to make sure that both routes could be completed within 2 hours. This time limit was set to minimize the spatial uncertainties in the data introduced by changes in the background weather conditions.



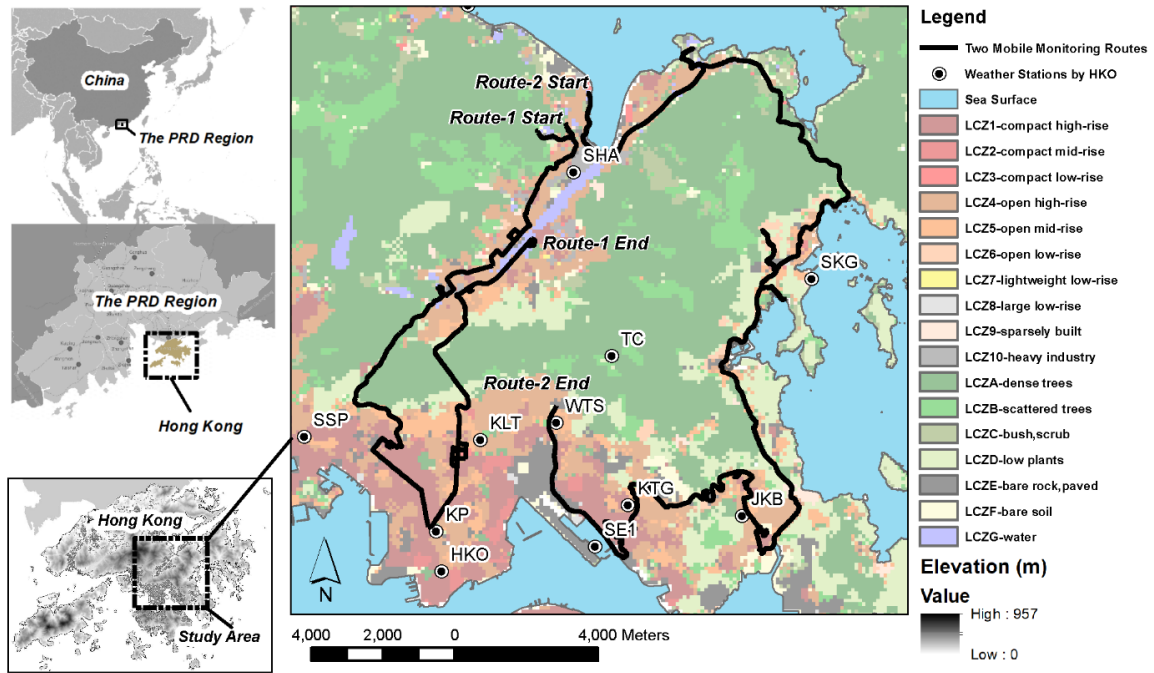


**Figure 3.** The two routes designed for the mobile measurement of the screen-level air temperature in different LCZ classes of Hong Kong.

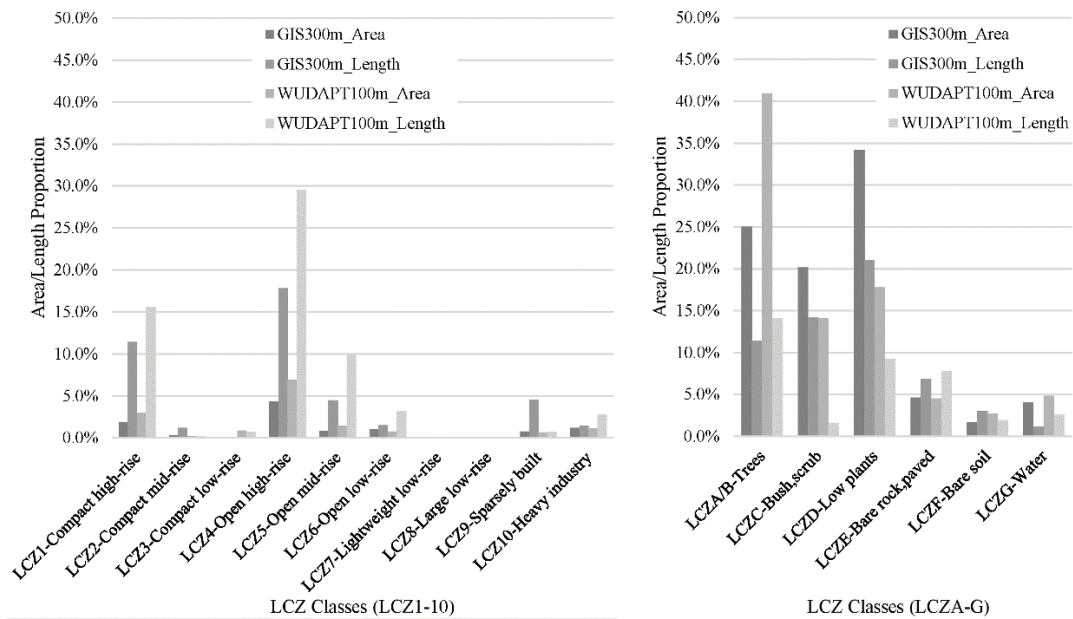


**Figure 4.** The areal proportion and corresponding composition of the route length in different LCZ classes.

A total of 12 runs of the mobile measurement were completed under the typical hot weather condition of Hong Kong (Table 3). The  $T_a$  and  $RH$  of the days for measurement

approximately ranged from 29°C to 34°C and 60% to 80% respectively. The sky condition measured as cloudiness (Oktas, 0-clear sky to 8-overcast) was also recorded. Three time periods of a day were measured to investigate the difference in the spatial variation in air temperature in different stages of a diurnal cycle.

**Table 3.** Summary of the meteorological conditions of the days during the mobile measurement. All data shown in this table are based on the weather records of the HKO meteorological stations (The time of sunset and sunrise during the survey dates are approximate 6:00 and 19:00. Run No.12 was a supplemental measurement because there was an instrumental error during the evening run on 27 Oct 2016. As shown in the table, the weather conditions of these two dates were similar).

Run No.	Date	Time Period	Routes	Air Temp. ( $T_a$ , °C)	Relative Humidity (RH, %)	Mean Wind Speed (v, m/s)	Sky Condition (Oktas)
1	17-Jul-16	09:00-11:00	Route-1	30.5-31.4	71-77	2.8	3
2	23-Jul-16	14:00-16:00	Route-1	32.1-32.4	64-66	3.8	3
3	23-Jul-16	19:00-21:00	Route-1	30.1-30.4	75-77	0.6	3
4	24-Aug-16	09:00-11:00	Route-1	29.8-31.3	65-70	1.9	4
5	24-Aug-16	14:00-16:00	Route-1	33.0-33.3	60-63	3.5	3
6	24-Aug-16	19:00-21:00	Route-1	29.4-29.9	75-81	3.5	3
7	25-Aug-16	09:00-11:00	Route-1	29.9-31.4	72-78	2.2	4
8	25-Aug-16	14:00-16:00	Route-1	33.9-34.3	63-64	3.4	2
9	25-Aug-16	19:00-21:00	Route-1	30.0-30.4	75-78	1.3	2
10	27-Oct-16	09:00-11:00	Route-2	28.9-29.7	73-81	1.9	5
11	27-Oct-16	14:00-16:00	Route-2	32.6-34.0	59-65	3.0	2
12	15-Aug-17	19:00-21:00	Route-2	29.3-30.0	73-75	1.4	2

### 2.3.3. Mobile Measurement Data Processing and Data Analysis

Although we have controlled the time period of each measurement to avoid significant background weather changes, the effect of temporal trend of  $T_a$  and  $RH$  should be removed from the spatially distributed data. As the meteorological data from HKO are only available on an hourly basis, we performed a linear detrending for each hour of the period of measurements to remove the temporal effect in the measurement data based on literature (Comrie 2000, Jonsson 2004). As shown in Figure 3, there are several HKO weather stations



1 close to the two measurement routes. Firstly, a 1Hz-temporally resolved linear trend was  
2 generated to represent the background weather changes at each station during each  
3 measurement run. Then, the 1Hz frequency-measured data points of  $T_a$  and  $RH$  were  
4 separated into different partitions based on their corresponding closest HKO weather station.  
5 Temporal correction was then conducted for each data partition using their corresponding  
6 time period based on the 1Hz-temporally resolved linear trend mentioned above. Based on  
7 the background meteorological records shown in Table 3, a day-to-day temporal correction  
8 was also performed to remove the temporal difference between the two mobile measurement  
9 routes.

10 To avoid the influence of the anthropogenic heat from vehicular exhaust, and to make the  
11 results of present study comparable with other LCZ/WUDAPT mobile measurement studies,  
12 all measurement data corresponding to a driving speed  $< 15$  km/h or  $> 60$ km were excluded  
13 from the dataset (the driving speed at each second was calculated in GIS). The driving speed  
14 criteria used here are consistent with a previous mobile measurement study in France  
15 (Leconte et al. 2015). Streets in Hong Kong, with its compact urban form, are often occupied  
16 by intense traffic and other activities. Under such context, some abnormal data points  
17 influenced by anomalous heat sources and sinks were observed in our measurement data.  
18 These abnormal data show up as spikes in the measurement data sequence. For example,  
19 there were abnormally high  $T_a$  observations (with a  $T_a > 35^\circ\text{C}$  lasting a few seconds during  
20 the nighttime measurement) caused by a suddenly passing-by heavy-duty truck or a double-  
21 decker bus emitting a large amount of the vehicular heat exhaust. We also observed some  
22 cool spots in the measurement data (with a  $T_a < 25^\circ\text{C}$  in the afternoon) caused by the cool  
23 airflow from the air conditioners in roadside shops. These data were screened out before  
24 further analysis was conducted. In this study, we used a median filter to remove the spikes  
25 mentioned above.

1 A median filter is a nonlinear filtering algorithm widely used for noise reduction in the data  
 2 sequence. It eliminates unwanted spikes in the signal without blurring any features of the  
 3 original data sequence (Huang, Yang, and Tang 1979). This makes the median filter a  
 4 suitable method for processing the mobile measurement data with inherent spatial  
 5 characteristics. A general 1-D median filter is shown as follows:  
 6  
 7  
 8  
 9  
 10

$$\hat{x}(n) = \text{median}[y(n - T), \dots, y(n - 1), y(n), y(n + 1), \dots, y(n + T)] \quad \text{Eq. 1}$$

11 where the median  $\hat{x}(n)$  was calculated within a moving window with the size of  $W = 2T + 1$ .  
 12 The spikes within the range of the moving window were detected by re-sorting the data in the  
 13 moving window and the out-of-range values were replaced by the calculated median  $\hat{x}(n)$ .  
 14 The moving window  $W$  slid along the entire data sequence to eliminate all suspected spikes.  
 15 To determine an appropriate  $W$  for the median filter of the mobile measurement data, all data  
 16 were imported into GIS for semivariogram ( $\hat{\gamma}$ ) modelling.  $\hat{\gamma}$  is defined as a function of  
 17 distance and shown as the following equation (O'Sullivan and Unwin 2014):  
 18  
 19  
 20  
 21  
 22  
 23  
 24  
 25  
 26  
 27  
 28  
 29  
 30  
 31  
 32  
 33

$$\hat{\gamma} = \frac{1}{2n(d)} \sum_{s_i - s_j = d} (T_{ai} - T_{aj})^2 \quad \text{Eq. 2}$$

34 All spatially distributed mobile measurement data points were paired ( $s_i$  and  $s_j$ ).  $d$  is the  
 35 distance between the two points of each pair.  $T_{ai}$  and  $T_{aj}$  are the observed  $T_a$  at  $s_i$  and  $s_j$ .  
 36  $n(d)$  is the total number of the pairs of all spatial points. As a function of  $d$ , the value of the  
 37 semivariogram continues to increase until a certain limit [usually defined as a value of 95%  
 38 of the sill,  $\sigma(0)$ ] at a certain distance of  $d = r$ . The  $r$  can be identified by fitting a  
 39 semivariogram curve using ordinary least squares (OLS). The number of the data points in a  
 40 corresponding circular area (with a diameter =  $r$ ) was used as the size  $W$  of the moving  
 41 window in the median filtering of the data sequence. At the end of the above process, the  
 42 unwanted data spikes caused by the random impacts were removed.  
 43  
 44  
 45  
 46  
 47  
 48  
 49  
 50  
 51  
 52  
 53  
 54  
 55  
 56  
 57  
 58  
 59  
 60  
 61  
 62  
 63  
 64  
 65

After the above preprocessing, all data were mapped in GIS combined with the GIS- and WUDAPT-based LCZ classification maps for further analysis. The present study concerns two kinds of differences/variations in  $T_a$  – differences between different LCZ classes ( $\Delta T_{a,LCZ X-LCZ Y}$ ) and the intra-LCZ variability ( $\sigma T_{a,LCZ X}$ ). The  $\Delta T_{a,LCZ X-LCZ Y}$  is defined as:

$$\Delta T_{a,LCZ X-LCZ Y} = |\overline{T_{a,LCZ X}} - \overline{T_{a,LCZ Y}}| \quad Eq. 3$$

where  $\Delta T_{a,LCZ X-LCZ Y}$  is the absolute difference of averaged  $T_a$  between LCZ X and LCZ Y.  $\overline{T_{a,LCZ X}}$  and  $\overline{T_{a,LCZ Y}}$  are the mean of the measured  $T_a$  in LCZ X and LCZ Y respectively. The  $T_{a,LCZ X}$  is defined as:

$$\overline{T_{a,LCZ X}} = \frac{1}{n} \sum_{i=1}^n T_{a,LCZ X_i} \quad Eq. 4$$

where  $n$  is the total number of all  $T_a$  data points measured in all area of the LCZ X.  $T_{a,LCZ X_i}$  is the measured value of  $T_a$  at the location  $i$  on the mobile measurement route. The  $\sigma T_{a,LCZ X}$  is defined as:

$$\sigma T_{a,LCZ X} = \sqrt{\frac{1}{n} \sum_{i=1}^n (T_{a,LCZ X_i} - \overline{T_{a,LCZ X}})^2} \quad Eq. 5$$

where  $\sigma T_{a,LCZ X}$  is the standard deviation of all  $T_a$  data points measured in LCZ X. A one-way analysis was performed for the processed  $T_a$  dataset mentioned earlier in this section by different LCZ classes. For the data of each LCZ class, the Analysis of Variance (ANOVA) test and Student's t test were performed to compare the average air temperatures in different LCZ classes ( $\overline{T_{a,LCZ X}}$ ,  $\overline{T_{a,LCZ Y}}$ , etc.). The above tests were also used to determine if there is any significant difference in the average air temperatures among LCZ classes (at a significant level of  $\alpha = 0.05$ ).

### 3. Results

#### 3.1. Mobile Measurement Data Analysis Results

The spatial variation of measured screen-level  $T_a$  and  $RH$  along the two measurement routes during daytime and nighttime is plotted in Figure 5. There were three time slots. The measurement periods of 9:00-11:00 and 14:00-16:00 were combined to represent daytime conditions; the period of 19:00-21:00 was used to reflect nighttime conditions. A considerable air temperature difference between high-density urban built-up area (LCZs 1 to 6) and other LCZ classes was observed. The highest temperature was observed in the high-density downtown area of Kowloon (mainly LCZ 1, LCZ 4. The bottom left part of the route map, near the HKO and KP weather stations). Relatively higher temperatures also appear in the Shatin new town in the New Territories (mainly LCZ4, close to the SHA weather station).

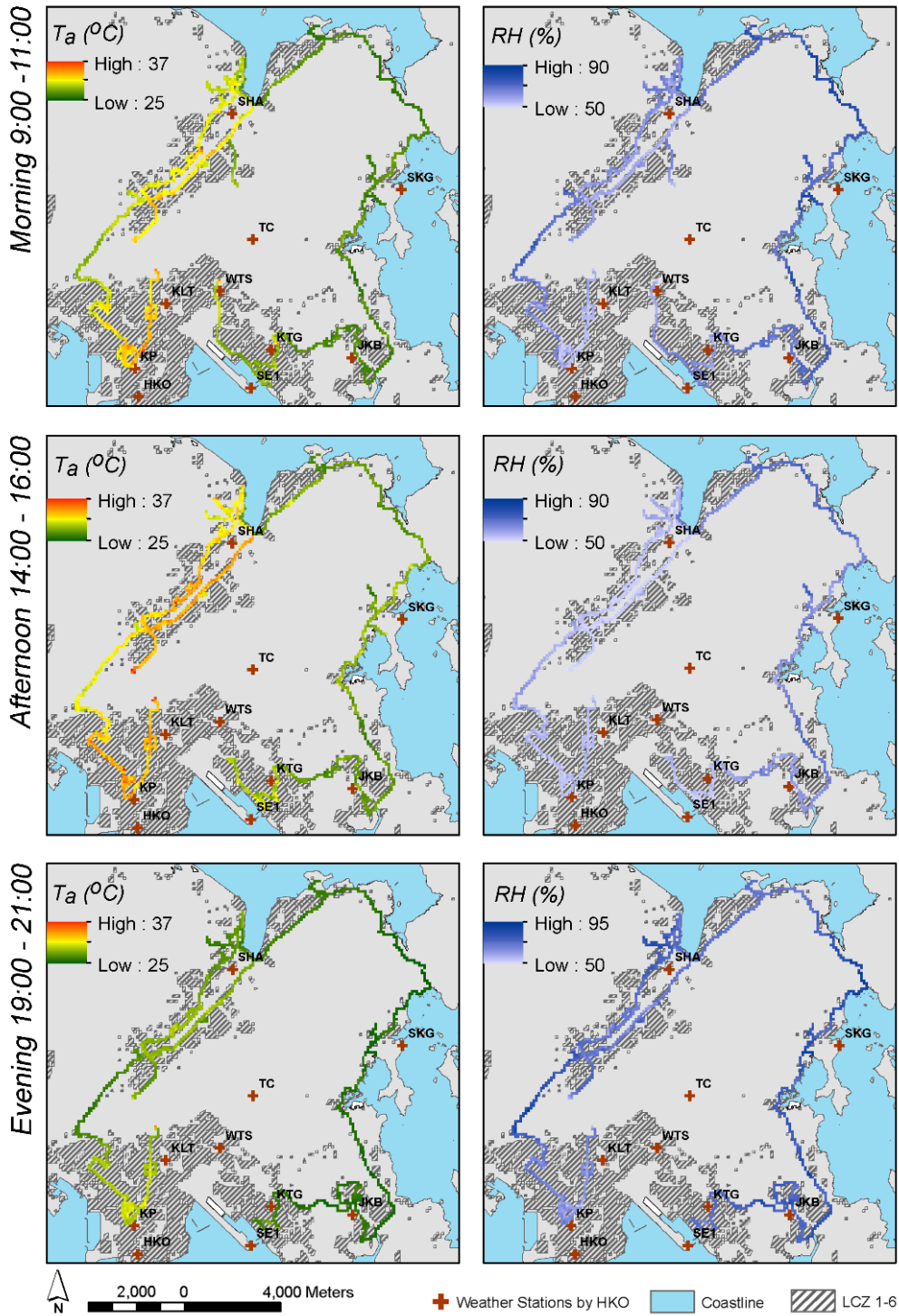


**Figure 5.** The spatial variation of measured screen-level  $T_a$  and RH along the two measurement routes during daytime and nighttime. (Figure S1-S3 in the supplementary material show the enlarged plots of the  $T_a$  panels).

Figure 6 shows the resultant semivariogram model and fitted curve based on the mobile measurement  $T_a$  data. The semivariogram reached 95% of the upper limit (the sill,  $\sigma(0)$ ) at a distance of approximately 340m. Therefore, this spatial scale was identified as an appropriate spatial scale to calculate the size of the moving window for the median filtering. The size of the moving window was determined to be 30 (because it takes an average of approximately 30s to pass through a distance of 340m during the mobile measurement campaigns).

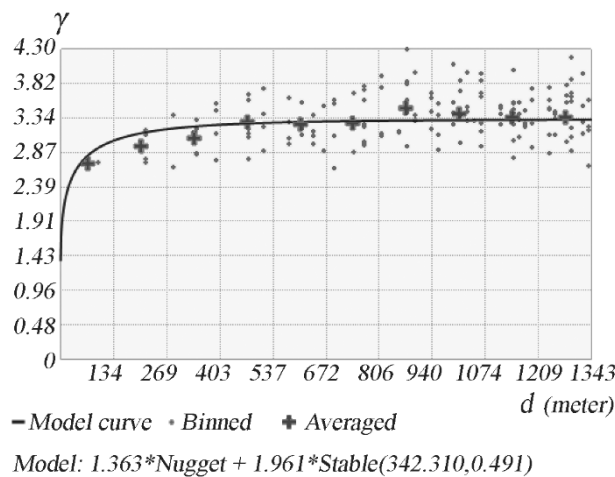


**Figure 6.** The resultant semivariogram model and the fitted curve based on the mobile measurement  $T_a$  data. The semivariogram reached 95% of the upper limit (the sill,  $\sigma(0)$ ) at a distance of 342.31m.

## 3.2. Air Temperature Difference and LCZ Classifications

### 3.2.1. Variation in Air Temperature among Different LCZ Classes

One-way analysis was performed for the  $T_a$  data by different LCZ classes based on both the 300m-resolution GIS-based LCZ map (Figure 7) and the 100m-resolution WUDAPT map (Figure 8) of Hong Kong. Both daytime and the nighttime  $T_a$  data were analyzed. For the data of each LCZ class, an Analysis of Variance (ANOVA) test was performed to calculate the  $\overline{T_{a,LCZ X}}$ . The Student's t test was performed to compare the  $\overline{T_{a,LCZ X}}$  of different LCZ classes (at a significant level of  $\alpha = 0.05$ ).

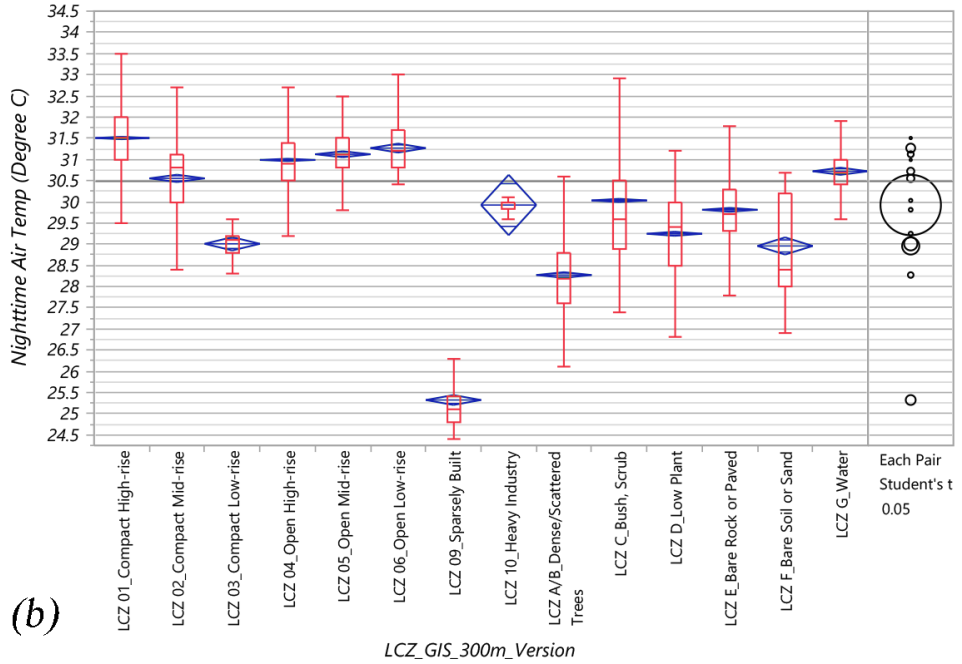
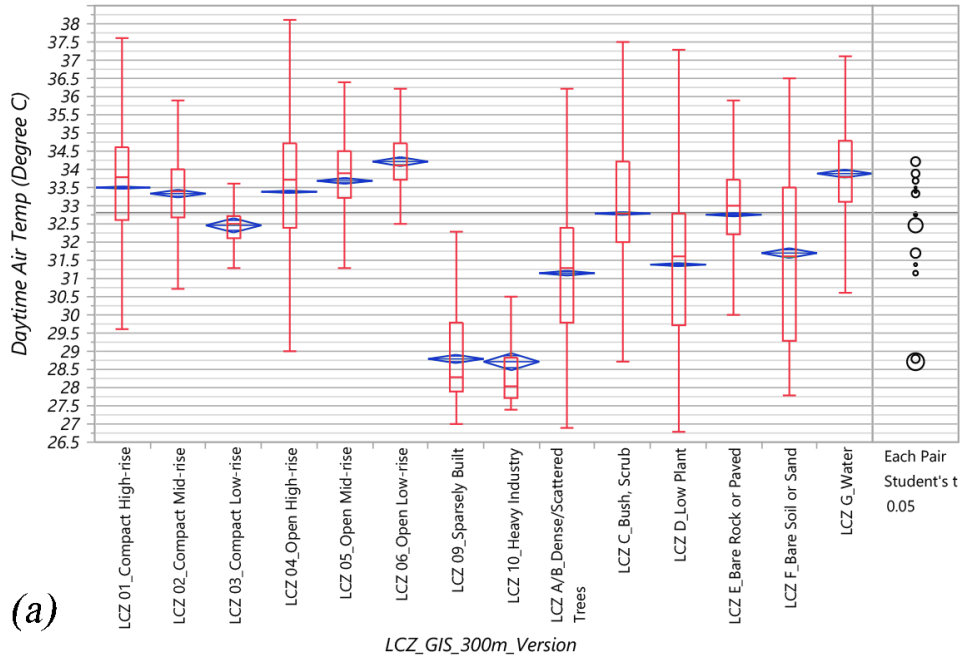


**Figure 7.** The one-way analysis result of the daytime (a) and nighttime air temperature (b) by the 300m-resolution GIS-based LCZ classification map.

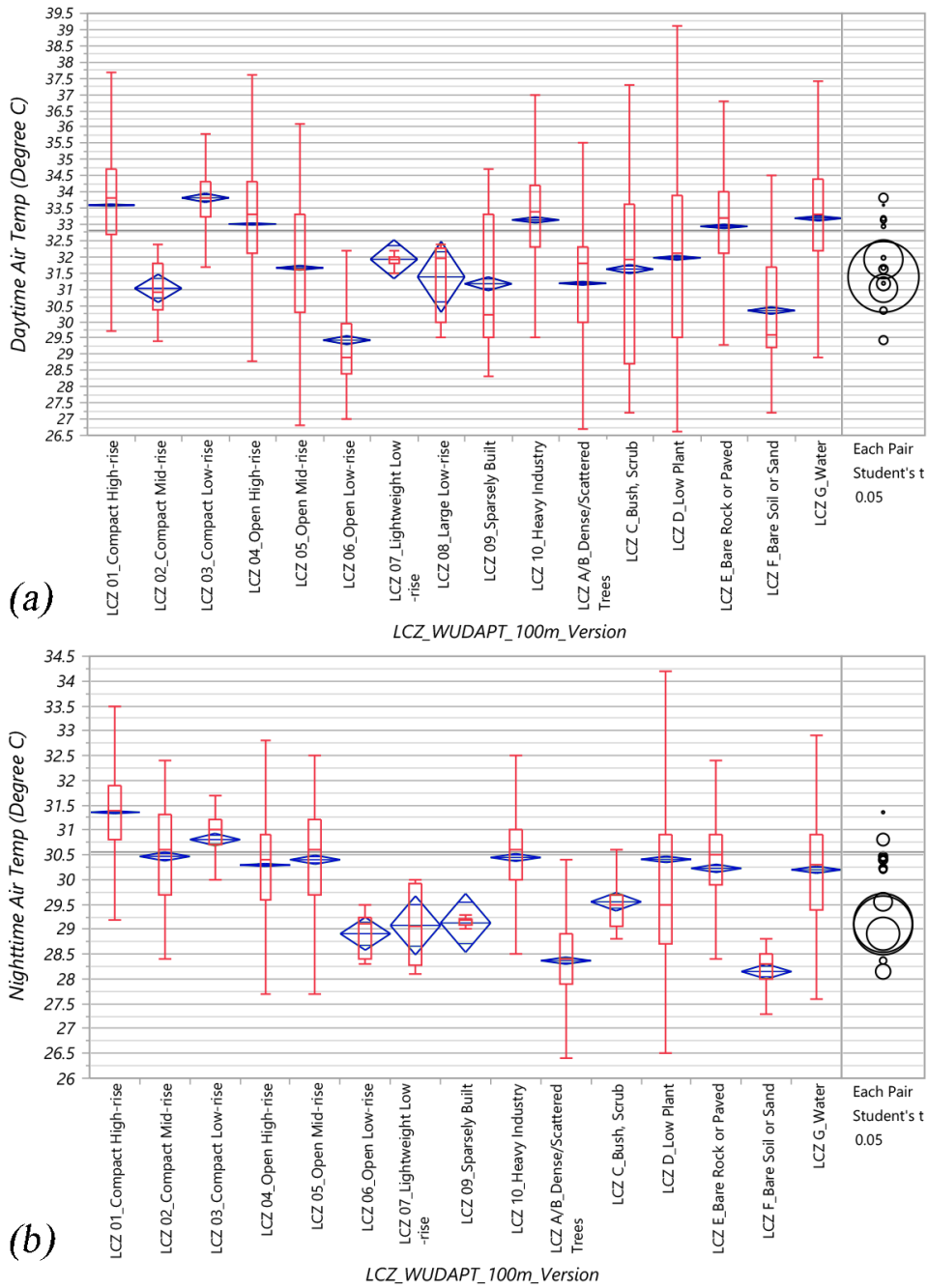


**Figure 8.** The one-way analysis result of the daytime (a) and nighttime air temperature (b) by the 100m-resolution WUDAPT method LCZ classification map.

A significant difference can be found in the air temperature between built-up classes (LCZ 1 to LCZ 10) and land cover classes (LCZ A to LCZ G) for both the GIS LCZ map and the WUDAPT map. It implies that both versions of LCZ classifications can well represent the urban-rural contrast in screen-level air temperature. The Student's t test results show that



there are significant  $T_a$  differences between most of the built-up classes (LCZ 1 to LCZ 10), which indicates that both versions of LCZ classification maps have successfully depicted the intra-urban air temperature difference (in the built-up area). In Hong Kong, the densely populated areas largely consist of six built-up classes, from LCZ 1 to LCZ 6 (labelled in Figure 3). Therefore, the present study paid more attention to these six classes due to their relevance to urban living. The ordered difference reports were prepared using the Student's t test for the daytime and nighttime air temperature differences based on two versions of the LCZ classification maps. As a result, the  $\Delta T_{a,LCZ X-LCZ Y}$  of each pair of LCZs 1 to 6 was calculated and shown in Figure 9 and Figure 10.

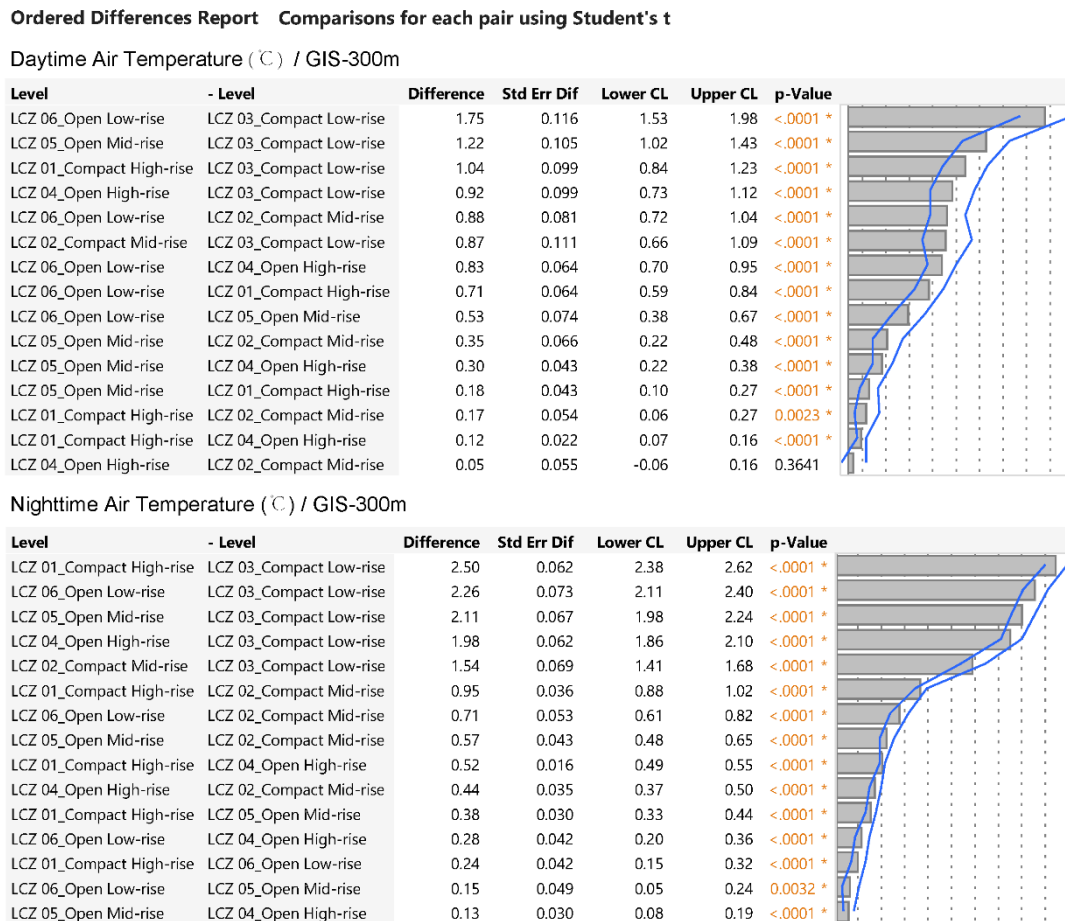


**Figure 9.** The ordered difference reports of the daytime and nighttime air temperature by the 300m-resolution GIS-based LCZ classification.

**Ordered Differences Report Comparisons for each pair using Student's t**

**Daytime Air Temperature (°C) / WUDAPT-100m**

Level	- Level	Difference	Std Err Dif	Lower CL	Upper CL	p-Value
LCZ 03_Compact Low-rise	LCZ 06_Open Low-rise	4.38	0.094	4.20	4.57	<.0001 *
LCZ 01_Compact High-rise	LCZ 06_Open Low-rise	4.16	0.067	4.03	4.29	<.0001 *
LCZ 04_Open High-rise	LCZ 06_Open Low-rise	3.58	0.067	3.45	3.71	<.0001 *
LCZ 03_Compact Low-rise	LCZ 02_Compact Mid-rise	2.79	0.225	2.35	3.23	<.0001 *
LCZ 01_Compact High-rise	LCZ 02_Compact Mid-rise	2.56	0.214	2.14	2.98	<.0001 *
LCZ 05_Open Mid-rise	LCZ 06_Open Low-rise	2.23	0.074	2.08	2.37	<.0001 *
LCZ 03_Compact Low-rise	LCZ 05_Open Mid-rise	2.16	0.076	2.01	2.31	<.0001 *
LCZ 04_Open High-rise	LCZ 02_Compact Mid-rise	1.98	0.214	1.56	2.40	<.0001 *
LCZ 01_Compact High-rise	LCZ 05_Open Mid-rise	1.93	0.036	1.86	2.00	<.0001 *
LCZ 02_Compact Mid-rise	LCZ 06_Open Low-rise	1.60	0.224	1.16	2.04	<.0001 *
LCZ 04_Open High-rise	LCZ 05_Open Mid-rise	1.35	0.036	1.28	1.42	<.0001 *
LCZ 03_Compact Low-rise	LCZ 04_Open High-rise	0.81	0.069	0.67	0.94	<.0001 *
LCZ 05_Open Mid-rise	LCZ 02_Compact Mid-rise	0.63	0.217	0.21	1.06	0.0036 *
LCZ 01_Compact High-rise	LCZ 04_Open High-rise	0.58	0.019	0.55	0.62	<.0001 *
LCZ 03_Compact Low-rise	LCZ 01_Compact High-rise	0.22	0.069	0.09	0.36	0.0012 *

**Nighttime Air Temperature (°C) / WUDAPT-100m**

Level	- Level	Difference	Std Err Dif	Lower CL	Upper CL	p-Value
LCZ 01_Compact High-rise	LCZ 06_Open Low-rise	2.45	0.142	2.17	2.72	<.0001 *
LCZ 03_Compact Low-rise	LCZ 06_Open Low-rise	1.90	0.151	1.60	2.19	<.0001 *
LCZ 02_Compact Mid-rise	LCZ 06_Open Low-rise	1.56	0.147	1.27	1.84	<.0001 *
LCZ 05_Open Mid-rise	LCZ 06_Open Low-rise	1.49	0.147	1.20	1.78	<.0001 *
LCZ 04_Open High-rise	LCZ 06_Open Low-rise	1.38	0.142	1.10	1.66	<.0001 *
LCZ 01_Compact High-rise	LCZ 04_Open High-rise	1.06	0.016	1.03	1.09	<.0001 *
LCZ 01_Compact High-rise	LCZ 05_Open Mid-rise	0.96	0.040	0.88	1.03	<.0001 *
LCZ 01_Compact High-rise	LCZ 02_Compact Mid-rise	0.89	0.039	0.81	0.97	<.0001 *
LCZ 01_Compact High-rise	LCZ 03_Open Low-rise	0.55	0.054	0.44	0.66	<.0001 *
LCZ 03_Compact Low-rise	LCZ 04_Open High-rise	0.51	0.054	0.41	0.62	<.0001 *
LCZ 03_Compact Low-rise	LCZ 05_Open Mid-rise	0.41	0.065	0.28	0.53	<.0001 *
LCZ 03_Compact Low-rise	LCZ 02_Compact Mid-rise	0.34	0.065	0.21	0.47	<.0001 *
LCZ 02_Compact Mid-rise	LCZ 04_Open High-rise	0.17	0.039	0.10	0.25	<.0001 *
LCZ 05_Open Mid-rise	LCZ 04_Open High-rise	0.11	0.040	0.03	0.19	0.0074 *
LCZ 02_Compact Mid-rise	LCZ 05_Open Mid-rise	0.07	0.054	-0.04	0.17	0.2190

**Figure 10.** The ordered difference reports of the daytime and nighttime air temperature by the 100m-resolution WUDAPT method LCZ classification.

**Table 4.** Summary of the pattern of air temperature differences among LCZs 1 to 6 based on the GIS-300m and WUDAPT-100m versions of the LCZ classification map of Hong Kong.

LCZ Classification	Daytime/ Nighttime	Summary of the pattern of air temperature differences among LCZs 1 to 6 <sup>a</sup>
GIS-300m	Daytime	$\overline{T_{a,LCZ 6}} > \overline{T_{a,LCZ 5}} > \overline{T_{a,LCZ 1}} > \overline{T_{a,LCZ 4}} \approx \overline{T_{a,LCZ 2}} > \overline{T_{a,LCZ 3}}$
GIS-300m	Nighttime	$\overline{T_{a,LCZ 1}} > \overline{T_{a,LCZ 6}} > \overline{T_{a,LCZ 5}} > \overline{T_{a,LCZ 4}} > \overline{T_{a,LCZ 2}} > \overline{T_{a,LCZ 3}}$
WUDAPT-100m	Daytime	$\overline{T_{a,LCZ 3}} > \overline{T_{a,LCZ 1}} > \overline{T_{a,LCZ 4}} > \overline{T_{a,LCZ 5}} > \overline{T_{a,LCZ 2}} > \overline{T_{a,LCZ 6}}$
WUDAPT-100m	Nighttime	$\overline{T_{a,LCZ 1}} > \overline{T_{a,LCZ 3}} > \overline{T_{a,LCZ 2}} \approx \overline{T_{a,LCZ 5}} > \overline{T_{a,LCZ 4}} > \overline{T_{a,LCZ 6}}$

a:  $\overline{T_{a,LCZ X}} > \overline{T_{a,LCZ Y}}$  indicates that the air temperature in LCZ X is significantly different from LCZ Y (higher).  
 $\overline{T_{a,LCZ X}} \approx \overline{T_{a,LCZ Y}}$  indicates that no statistically significant air temperature difference was found between LCZ X and LCZ Y.

1  
2  
3  
4  
5  
6  
7  
8  
9  
10  
11  
12  
13  
14  
15  
16  
17  
18  
19  
20  
21  
22  
23  
24  
25  
26  
27  
28  
29  
30  
31  
32  
33  
34  
35  
36  
37  
38  
39  
40  
41  
42  
43  
44  
45  
46  
47  
48  
49  
50  
51  
52  
53  
54  
55  
56  
57  
58  
59  
60  
61  
62  
63  
64  
65

By comparing the above results of LCZ 1 to LCZ 6 (Table 4), some common findings about air temperature differences can be summed up:

(1) LCZ 1 compact high-rise area has the highest air temperature during nighttime. It is approximately 0.9°C higher than the LCZ 2 compact mid-rise area and 0.5 - 1.1°C higher than the LCZ 4 open high-rise area. This result is similar to other cities and within our expectation. The compactly arranged buildings in LCZ 1 slow down the night heat dissipation process.

(2) During daytime, the  $T_a$  differences between LCZ 1, LCZ 2, and LCZ 3 are commonly smaller than those during nighttime. The GIS-based results show that the pattern of  $\overline{T_{a,LCZ 1}} > \overline{T_{a,LCZ 2}} > \overline{T_{a,LCZ 3}}$  remains unchanged across the day.

(3)  $\Delta T_{a,LCZ 2-LCZ 4}$  and  $\Delta T_{a,LCZ 2-LCZ 5}$  are relatively small, indicating that besides the urban morphological indicators used in the LCZ classification system, there are other underlying variables that have an influence on the screen-level air temperature in the complex geographic setting of Hong Kong. These underlying influential variables include but are not limited to relief, terrain, proximity to water bodies, rural soil moisture, sea breeze, unevenly distributed anthropogenic heat sources, and highly heterogeneous vegetation species, etc.

(4) The GIS-based results also indicate that  $\overline{T_{a,LCZ 6}}$  and  $\overline{T_{a,LCZ 5}}$  are higher than  $\overline{T_{a,LCZ 4}}$  and  $\overline{T_{a,LCZ 1}}$  during daytime. During daytime, the total incoming solar radiation in LCZ 5 and LCZ 6 is much larger than LCZ 1 and LCZ 4 because of less shading. Similarly, relatively high daytime air temperature is also observed in other cases (Quanz et al. 2018, Skarbit et al. 2017). It should be noted that, the situation could vary between different cities. It is highly dependent on their individual latitudes (which can affect the amount of incoming solar radiation) and climate types (which can lead to different levels of the temperature variation between day and night), etc. The above further confirms the significance of shadings in the

1 improvement of screen-level thermal environment under the meteorological condition of  
2 subtropical cities, such as Hong Kong.  
3

4  
5 However, the pattern of  $\overline{T_{a,LCZ 6}} / \overline{T_{a,LCZ 5}} > \overline{T_{a,LCZ 4}} / \overline{T_{a,LCZ 1}}$  does not appear in the  
6  
7 WUDAPT-based results. It can be attributed to the fundamental difference between the two  
8  
9 classification methods. The GIS-based method largely depends on real morphological  
10  
11 features while the WUDAPT method is a workflow basing entirely on Landsat imagery and  
12  
13 random forest classification scheme (Mills et al. 2015). In the WUDAPT method, radiation  
14  
15 could be a significant factor because it affects the remote sensing signal in different spectral  
16  
17 bands of the satellite images. Significant differences have been observed between GIS and  
18  
19 WUDAPT results in the  $T_a$  of LCZ 6 in both daytime and nighttime. The  $T_a$  of WUDAPT  
20  
21 LCZ 6 is much lower than GIS LCZ 6 because many sparsely-built villages (LCZ 9 sites in  
22  
23 the GIS-based LCZ map) with a low  $T_a$  in the coastal area of Sai Kung were mistaken as LCZ  
24  
25 6 by the WUDAPT classification. There are also noticeable differences in the nighttime  $T_a$  of  
26  
27 LCZ 3 because many open low-rise areas (LCZ 6 sites in the GIS-based LCZ map) were  
28  
29 identified as the LCZ 3 by the WUDAPT classification. The above observation implies that  
30  
31 the criteria for the determination of the compactness of low-rise areas should be further  
32  
33 refined in WUDAPT. In other words, it is important to differentiate between “compact” and  
34  
35 “open” more accurately. The pattern of  $T_a$  in LCZ7 - LCZ9 is not stable because the areas of  
36  
37 these LCZ classes are extremely small in Hong Kong (as mentioned earlier in section 2.2.1).  
38  
39  
40  
41  
42  
43  
44  
45  
46

### 47 **3.2.2. Intra-LCZ Variability**

48  
49 The  $\sigma T_{a,LCZ X}$  of each LCZ class was calculated (Table 5). The results show that all daytime  
50  
51  $\sigma T_{a,LCZ X}$  are approximately two times larger than nighttime, because of the influence of solar  
52  
53 radiation. To be more specific, even in a high-density urban context with a homogeneous  
54  
55 morphological form, the incoming shortwave solar radiation is still unevenly distributed at  
56  
57  
58  
59  
60  
61  
62  
63  
64  
65

different locations due to the complicated shading of the densely constructed building clusters.

It further leads to considerable spatial variability in screen-level air temperatures. The above spatial variabilities have been observed in the urban context of Hong Kong in a previous study (Shi et al. 2015). In that study, the spatial distribution of daytime screen-level air temperature was separately measured in the two study areas of Tsim Sha Tsui, Kowloon (mainly LCZ 1) and Tai Po, New Territories (LCZ 5 and LCZ 2). A range (measured as the  $T_{a,max,LCZ X} - T_{a,min,LCZ X}$ ) of up to 2°C was measured in both study areas (Figure 11).

Moreover, the pattern of  $\sigma T_{a,LCZ 1} > \sigma T_{a,LCZ 2} > \sigma T_{a,LCZ 3}$  does not change across daytime and nighttime, which further proves the influence of the shading effect of high-rise buildings on the intra-LCZ variability of screen-level air temperature.

**Table 5.** Summary of the intra-LCZ variability of air temperature ( $\sigma T_{a,LCZ X}$ , °C) in LCZ 1 to LCZ 6 based on the GIS-300m and WUDAPT-100m versions of the LCZ classification map of Hong Kong.

LCZ Class (LCZ 1 to LCZ 6)	Indicator (°C)	GIS-300m version		WUDAPT-100m version	
		Daytime	Nighttime	Daytime	Nighttime
LCZ 01 Compact High-rise	$\sigma T_{a,LCZ 1}$	1.89	0.79	1.74	0.90
LCZ 02 Compact Mid-rise	$\sigma T_{a,LCZ 2}$	1.31	0.88	0.82	1.00
LCZ 03 Compact Low-rise	$\sigma T_{a,LCZ 3}$	0.66	0.31	1.19	0.66
LCZ 04 Open High-rise	$\sigma T_{a,LCZ 4}$	1.97	0.81	2.02	1.00
LCZ 05 Open Mid-rise	$\sigma T_{a,LCZ 5}$	1.45	0.61	2.05	1.06
LCZ 06 Open Low-rise	$\sigma T_{a,LCZ 6}$	0.75	0.49	1.49	0.41

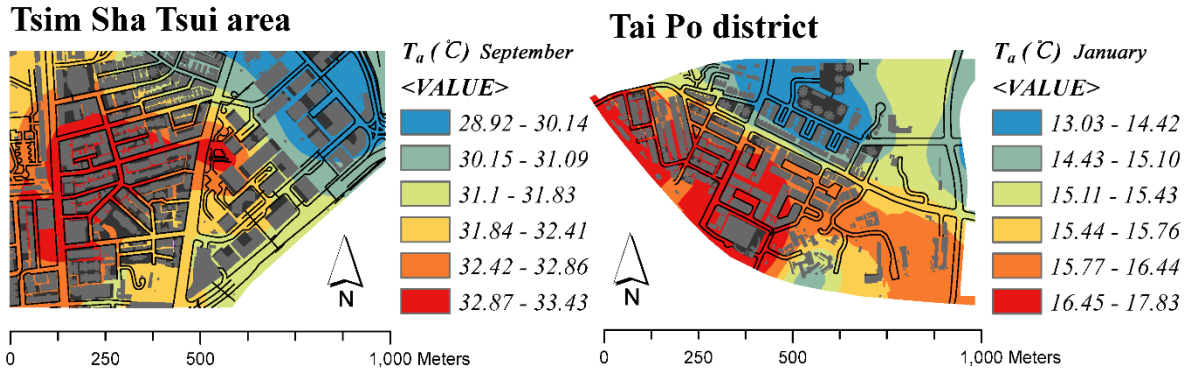


**Figure 11.** The daytime screen-level air temperature in the two study areas respectively.

Modified from Shi et al. (2015).

By comparing the  $\sigma T_{a,LCZ X}$  (LCZ 1 to LCZ 6) calculated based on the two different versions of LCZ classification maps, it was found that the GIS-300m version of LCZ classification map produced a much smaller  $\sigma T_{a,LCZ 3}$ ,  $\sigma T_{a,LCZ 6}$  than the WUDAPT-100m version (almost 50% smaller). The smaller  $\sigma T_{a,LCZ X}$  in low-rise building areas indicates that the GIS-based LCZ classification method provides a more accurate classification for these areas than WUDAPT. The reason is that the GIS-based method involves a large amount of precise building data from surveying. Such data are not used in the current WUDAPT method. However, it was also found that both the GIS-300m and WUDAPT-100m LCZ classification maps produce a relatively large  $\sigma T_{a,LCZ 1}$ ,  $\sigma T_{a,LCZ 4}$  of 1.8 – 2.0°C and a  $\sigma T_{a,LCZ 2}$ ,  $\sigma T_{a,LCZ 5}$  of 1.3 – 2.0°C. The above  $\sigma T_{a,LCZ X}$  is already larger than many of the  $\Delta T_{a,LCZ X-LCZ Y}$  (refers to the Figure 9 and Figure 10). The results of  $\sigma T_{a,LCZ X} > \Delta T_{a,LCZ X-LCZ Y}$  reveal that there are still other influential variables of screen-level air temperature that are not being considered in the current two versions of LCZ classification maps of Hong Kong (as indicated, for example, the unevenly distributed anthropogenic heat sources, heterogeneous vegetation species, and influence of incoming solar radiation). It has been clearly identified that the dominant microclimate impact factors are different across LCZ sites (Shi et al. 2015). Taking the two LCZ sample sites shown in Figure 11 as an example, we identified that the

1 dominant effect of air temperature in the Tsim Sha Tsui site (LCZ 1) was building  
2 morphology (measured as SVF). In contrast, urban greening and the surrounding vegetated  
3 mountainous topography were more influential in the air temperature in the Tai Po site (LCZ  
4 2 and LCZ 5). Therefore, the effects of complex terrain, relief, water bodies, soil moisture,  
5 etc. are also parts of the influencing factors of the observed intra-LCZ variability of air  
6 temperature of Hong Kong. A similar micro-scale variability of air temperature was also  
7 observed in other cases (Quanz et al. 2018). They need to be taken into consideration in  
8 further LCZ/WUDAPT urban climate research.  
9

### 20 **3.2.3. Influencing Building Morphological Factors of Air Temperature**

21 It has been found that building morphology has a considerable influence on the intraurban  
22 spatial variability of air temperature, especially in the high-density urban context of Hong  
23 Kong (Shi, Katzschner, and Ng 2018). In the present study, a multivariate analysis was  
24 performed in order to identify the most important building morphological factors of the  
25 intraurban variability of air temperature. To be more specific, a series of correlation analysis  
26 between the site-averaged daytime/nighttime air temperature and the three building  
27 morphological factors -  $\lambda_b$ ,  $Z_h$ ,  $\Psi_{svf}$  (adopted in the LCZ classification process of this study;  
28 Section 2.2.1) were conducted. The results (Table 6) show that both the  $Z_h$  and  $\Psi_{svf}$  have a  
29 significant correlation with site averaged temperature. The influence of building morphology  
30 on air temperature is even stronger during nighttime. The influence of  $\Psi_{svf}$  on the urban air  
31 temperature differences has been indicated by local researchers (Chen et al. 2012), and  
32 further validated by the LCZ scheme and mobile measurement data in this study.  
33  
34  
35  
36  
37  
38  
39  
40  
41  
42  
43  
44  
45  
46  
47  
48  
49  
50  
51  
52  
53  
54  
55  
56  
57  
58  
59  
60  
61  
62  
63  
64  
65

**Table 6.** The Pearson Correlation Coefficient ( $R$ ) between the LCZ site-averaged air temperature and building morphological parameters.

	Building surface fraction ( $\lambda_b$ )	Building height ( $Z_h$ )	Sky view factor ( $\Psi_{svf}$ )
Daytime air temperature ( $T_{a,daytime}$ )	0.14	0.34	-0.33
Nighttime air temperature ( $T_{a,nighttime}$ )	0.33	0.48	-0.47

#### 4. Discussion and Conclusions

##### 4.1. GIS-based Method and WUDAPT Method of LCZ Classification in the High-density Urban Scenario

The LCZ classification mapping study of Hong Kong is one of the first applications of the LCZ system in such an extremely compact and high-density urban scenario under the subtropical climatic condition. It has been reported by some researchers that the LCZ scheme is not always suitable for the Asian cities due to their unique urban contexts and the combination of land-use and building morphology. They commented that the criteria should be slightly modified to adapt to the local context (Kotharkar and Bagade 2017). However, the above concern does not seem to materialize in the present study. Although the built-up areas of Hong Kong are extremely dense, the standard morphological values of LCZ classes proposed by Stewart and Oke (2012) were strictly followed during the classification process. In the present study, no modification was made to the classification criteria. However, there are still certain advantages and disadvantages of using the two LCZ mapping methods. Table 7 provides a brief discussion about the limitation and potential of the two methods for future urban climate studies. It could be expected that a combination of both methods would provide a more robust and accurate LCZ classification/map for further urban climatic research.



**Table 7.** A brief summary of the advantages and disadvantages of GIS-based and WUDAPT method for LCZ classification mapping in high-density urban scenario.

	<b>GIS-based Method</b>	<b>WUDAPT Method</b>
<b>Input data requirement</b>	This method has a high requirement for the input datasets. It requires comprehensive and high-quality urban land use and building surveying datasets from local authorities, which might not always be available.	All required data, software and generated results of WUDAPT are free and can be publicly accessed. It makes this method work well with the lack of precise urban morphology data. The feasibility of this method is high.
<b>Classification Criteria/Procedure</b>	Different cities may have different classification criteria/procedures, depending on their own reality of urban scenario and data availability. In some cases, the original LCZ scheme has to be slightly modified/adjusted based on the local context in order to avoid "unclassified areas".	The WUDAPT method strictly follows a standardized working procedure for data collection and data processing. The method takes the advantages of machine-learning and remote-sensing technology. The whole working procedure ensures a high working efficiency and makes the automation process possible.
<b>Spatial resolution of outputs</b>	The spatial resolution of the resultant GIS-based LCZ maps usually ranges from 200m to 500m depending on the local context/situations. Sensitivity tests are usually required to determine a suitable resultant spatial resolution. The spatial resolution of 200-500 m for the GIS method is a suitable scale for local climate studies.	A unified global standard spatial resolution – 100m was used, which could be a big advantage in the integration/collation of the LCZ data from different cities/regions. It is also an ideal data platform for intercity cross comparison studies and other worldwide collaboration research.
<b>The accuracy of the classification results</b>	High accuracy could be expected because the method takes full advantages of the accurate, comprehensive and detailed urban datasets from local authorities. The standard values proposed by the LCZ scheme and the application of GIS produce more objective and robust results. At the district level, the GIS-based method detects more urban form details than the WUDAPT method. The GIS results are more detailed/accurate than the WUDAPT results in investigating urban built-up areas (LCZs 1 to 6).	The accuracy of the resultant classification highly depends on the selection of training samples. The subjective artificial visual interpretation method may introduce certain biases/errors to the classification results. Well-trained experts with a good understanding of local urban context must be involved to ensure the classification accuracy. However, the WUDAPT method classifies land cover types more accurately because it employs remote-sensing technology.
<b>Potential applications</b>	Urban planning/design optimization; Site selection for UHI and microscale urban climate/thermal comfort studies. Etc.	Enhanced Input dataset for improving the mesoscale and region scale weather forecast and climatic modelling. Etc.

## 4.2. Evaluating the Current LCZ/WUDAPT Mappings of Hong Kong by Mobile

### Measurement

The current LCZ/WUDAPT mappings in Hong Kong were evaluated by mobile measurement campaigns. Significant variations in air temperature between different LCZ classes were observed. In the present study, the mobile measurement campaigns have overcome the

1 monitoring gaps of sparsely distributed fixed weather stations and provide more  
2 comprehensive spatial information of screen-level air temperature at a finer spatial scale. By  
3  
4 investigating the actual measured data from the mobile measurement, this study illustrates  
5  
6 that both the urban-rural contrast and differences in screen-level air temperature between  
7  
8 LCZ classes can be appropriately depicted for Hong Kong by using the current LCZ maps  
9  
10 (both the GIS-300m and WUDAPT-100m versions). The study results evaluate the usefulness  
11  
12 of the LCZ classification mapping for Hong Kong in delivering reliable data to urban climate  
13  
14 researchers as well as local planners and architects. By classifying the urban morphological  
15  
16 variables, land use, and surface properties that directly influence the spatial variability of  
17  
18 screen-level air temperature (such as building height, ground coverage ratio, sky view factors,  
19  
20 and the fraction of vegetation), the two current LCZ maps are readily applicable for further  
21  
22 local urban climate research.  
23  
24  
25  
26  
27  
28  
29

### 30 **4.3. Limitations**

31  
32 The effects of atmospheric mixing could vary under different synoptic types. There are only a  
33  
34 limited number of the measurements in the present study, and more measurement campaigns  
35  
36 should be conducted to cover different weather/synoptic types of Hong Kong. In addition, it  
37  
38 needs to be recognized that the effects of complex terrain, relief, water bodies, soil moisture,  
39  
40 etc. are also parts of the influencing factors of the observed inter- and intra-LCZ variability of  
41  
42 air temperature of Hong Kong. However, the heterogeneous and complex geography of Hong  
43  
44 Kong means that the above effects vary from site to site. Hence, they are difficult to be fully  
45  
46 investigated in one single study. Further investigations need to be conducted by selecting  
47  
48 locally representative sites within the LCZ classes such as what has been done by Bokwa et al.  
49  
50 (2015). Last but not the least, the current study still focusses on the LCZ/WUDAPT mapping.  
51  
52 Therefore, the priority was given to the spatial coverage of the measurement data. In order to  
53  
54  
55  
56  
57  
58  
59  
60  
61  
62  
63  
64  
65

1 improve the representativeness of the data, follow-up work should also focus on improving  
2 the mobile measurement and data extraction methods.  
3  
4

#### 5 **4.4. Future Work - Dealing with the Intra-LCZ Variability**

6

7  
8  
9 The intra-LCZ variability caused by the high-density heterogeneous urban environment was  
10 observed by this study, especially in LCZ 1 to LCZ 6. It implies that further refinement of the  
11 classification method/mapping procedure is necessary to improve the classification accuracy  
12 for both the GIS-based and WUDAPT methods. Bokwa et al. (2015) have conducted an in-  
13 depth study on the investigation of the influence of relief on the urban air temperature.  
14  
15  
16  
17  
18  
19

20  
21 Similar investigations are highly necessary in Hong Kong. In the future, WUDAPT level 1 &  
22 2 data should be considered, since they can provide complete coverage of the urban  
23 landscape and include information of individual building elements and features (Xu et al.  
24 2017).  
25  
26  
27  
28  
29  
30

31 Intra-LCZ variability is also important to urban planning and design because environmental  
32 diversity is an important element in improving the environmental quality of urban areas. A  
33 diverse urban environment provides a wide range of thermal environments that accommodate  
34 different needs of urban dwellers (Lau, Lindberg, et al. 2015). It also allows for a wider  
35 choice of planning measures to mitigate the heat island effect. Therefore, future work should  
36 focus on the interpretation of the classification maps based on the underlying influential  
37 variables of screen-level air temperature mentioned above. Further adjustments and  
38 refinements based on the unique local situation/context could provide better  
39 information/reference for future urban climate studies. Considering the aforementioned  
40 limitations of the present study, future work should also focus on the improvement of the  
41 mobile measurement method and extraction of reliable and representative temperature data.  
42  
43  
44  
45  
46  
47  
48  
49  
50  
51  
52  
53  
54  
55  
56  
57  
58  
59  
60  
61  
62  
63  
64  
65

## ACKNOWLEDGEMENT

This research is supported by the General Research Fund (GRF Project No.: 14643816 and 14629516) from the Research Grants Council (RGC) of Hong Kong. The authors deeply thank the reviewers for their insightful comments, feedbacks and constructive suggestions, recommendations on our research work. The authors also want to appreciate editors for their patient and meticulous work for our manuscript. The authors also thank Ms. Ada Lee of the Chinese University of Hong Kong for her kind help on this paper.

## REFERENCES

- Alexander, Paul, and Gerald Mills. 2014. "Local Climate Classification and Dublin's Urban Heat Island." *Atmosphere* no. 5 (4):755.
- Bechtel, Benjamin, Paul Alexander, Jürgen Böhner, Jason Ching, Olaf Conrad, Johannes Feddema, Gerald Mills, Linda See, and Iain Stewart. 2015. "Mapping Local Climate Zones for a Worldwide Database of the Form and Function of Cities." *ISPRS International Journal of Geo-Information* no. 4 (1):199.
- Betanzo, Miko. 2007. "Pros and cons of high density urban environments." *Build, April/May*:39-40.
- Blankenstein, Simone, and Wilhelm Kuttler. 2004. "Impact of street geometry on downward longwave radiation and air temperature in an urban environment." *Meteorologische Zeitschrift* no. 13 (5):373-379. doi: 10.1127/0941-2948/2004/0013-0373.
- Bokwa, Anita, Monika J. Hajto, Jakub P. Walawender, and Mariusz Szymanowski. 2015. "Influence of diversified relief on the urban heat island in the city of Kraków, Poland." *Theoretical and Applied Climatology* no. 122 (1):365-382. doi: 10.1007/s00704-015-1577-9.
- Chan, Emily Ying Yang, William B Goggins, Jacqueline Jakyounng Kim, and Sian M Griffiths. 2012. "A study of intracity variation of temperature-related mortality and socioeconomic status among the Chinese population in Hong Kong." *Journal of epidemiology and community health* no. 66 (4):322-327.
- Chen, Liang, Edward Ng, Xipo An, Chao Ren, Max Lee, Una Wang, and Zhengjun He. 2012. "Sky view factor analysis of street canyons and its implications for daytime intra-urban air temperature differentials in high-rise, high-density urban areas of Hong

- 1 Kong: a GIS-based simulation approach." *International Journal of Climatology* no. 32  
2 (1):121-136. doi: 10.1002/joc.2243.
- 3  
4 Comrie, Andrew C. 2000. "Mapping a Wind-Modified Urban Heat Island in Tucson, Arizona  
5 (with Comments on Integrating Research and Undergraduate Learning)." *Bulletin of*  
6 *the American Meteorological Society* no. 81 (10):2417-2431. doi: 10.1175/1520-  
7 0477(2000)081<2417:mawmuh>2.3.co;2.
- 8  
9  
10 Davenport, Alan G, C Sue B Grimmond, Tim R Oke, and Jon Wieringa. 2000. Estimating the  
11 roughness of cities and sheltered country. Paper read at Proceedings 12th Conference  
12 on Applied Climatology, Asheville, NC, American Meteorological Society, Boston.
- 13  
14  
15 Eliasson, Ingegärd. 1990. "Urban Geometry, surface temperature and air temperature."  
16 *Energy and Buildings* no. 15 (1):141-145. doi: [http://dx.doi.org/10.1016/0378-](http://dx.doi.org/10.1016/0378-7788(90)90125-3)  
17 [7788\(90\)90125-3](http://dx.doi.org/10.1016/0378-7788(90)90125-3).
- 18  
19  
20  
21 Eliasson, Ingegärd. 2000. "The use of climate knowledge in urban planning." *Landscape and*  
22 *urban planning* no. 48 (1):31-44.
- 23  
24  
25 Grimmond, S. U. E. 2007. "Urbanization and global environmental change: local effects of  
26 urban warming." *Geographical Journal* no. 173 (1):83-88. doi: 10.1111/j.1475-  
27 4959.2007.232\_3.x.
- 28  
29  
30  
31 Hedquist, Brent C., and Anthony J. Brazel. 2006. "Urban, Residential, and Rural Climate  
32 Comparisons from Mobile Transects and Fixed Stations: Phoenix, Arizona." *Journal*  
33 *of the Arizona-Nevada Academy of Science* no. 38 (2):77-87. doi: 10.2181/1533-  
34 6085(2006)38[77:URARCC]2.0.CO;2.
- 35  
36  
37  
38 Huang, T., G. Yang, and G. Tang. 1979. "A fast two-dimensional median filtering  
39 algorithm." *IEEE Transactions on Acoustics, Speech, and Signal Processing* no. 27  
40 (1):13-18. doi: 10.1109/TASSP.1979.1163188.
- 41  
42  
43  
44 IPCC. 2014. *Climate Change 2014—Impacts, Adaptation and Vulnerability: Regional Aspects*.  
45 Cambridge, United Kingdom and New York, NY, USA: Cambridge University Press.
- 46  
47  
48  
49  
50  
51  
52  
53  
54  
55  
56  
57  
58  
59  
60  
61  
62  
63  
64  
65

- 1  
2 Kotharkar, Rajashree, and Anurag Bagade. 2018. "Evaluating urban heat island in the critical  
3 local climate zones of an Indian city." *Landscape and Urban Planning* no. 169:92-  
4 104. doi: <http://dx.doi.org/10.1016/j.landurbplan.2017.08.009>.
- 5 Landsberg, Helmut E. 1981. *The urban climate*. Vol. 28. London: Academic press.
- 6  
7 Lau, Kevin Ka-Lun, Fredrik Lindberg, David Rayner, and Sofia Thorsson. 2015. "The effect  
8 of urban geometry on mean radiant temperature under future climate change: a study  
9 of three European cities." *International Journal of Biometeorology* no. 59 (7):799-814.  
10 doi: 10.1007/s00484-014-0898-1.
- 11  
12 Lau, Kevin Ka-Lun, Chao Ren, Yuan Shi, Venessa Zheng, Steve Yim, and Derrick Lai. 2015.  
13 Determining the optimal size of local climate zones for spatial mapping in high-  
14 density cities. In *9th International Conference on Urban Climate jointly with 12th*  
15 *Symposium on the Urban Environment*,. Toulouse, France: International Association  
16 for Urban Climate (IAUC) and American Meteorological Society (AMS).
- 17  
18 Leconte, Francois, Julien Bouyer, Rémy Claverie, and Mathieu Pétrissans. 2015. "Using  
19 Local Climate Zone scheme for UHI assessment: Evaluation of the method using  
20 mobile measurements." *Building and Environment* no. 83:39-49. doi:  
21 <http://dx.doi.org/10.1016/j.buildenv.2014.05.005>.
- 22  
23 Lehnert, Michal, Jan Geletič, Jan Husák, and Miroslav Vysoudil. 2015. "Urban field  
24 classification by "local climate zones" in a medium-sized Central European city: the  
25 case of Olomouc (Czech Republic)." *Theoretical and Applied Climatology* no. 122  
26 (3):531-541. doi: 10.1007/s00704-014-1309-6.
- 27  
28 Liu, Lin, Yaoyu Lin, Dan Wang, and Jing Liu. 2016. "An improved temporal correction  
29 method for mobile measurement of outdoor thermal climates." *Theoretical and*  
30 *Applied Climatology*:1-12. doi: 10.1007/s00704-016-1769-y.
- 31  
32 Loridan, Thomas, and C. S. B. Grimmond. 2012. "Characterization of Energy Flux  
33 Partitioning in Urban Environments: Links with Surface Seasonal Properties."  
34 *Journal of Applied Meteorology and Climatology* no. 51 (2):219-241. doi:  
35 10.1175/jamc-d-11-038.1.
- 36  
37 Loridan, Thomas, Fredrik Lindberg, Oriol Jorba, Simone Kotthaus, Susanne Grossman-  
38 Clarke, and C. S. B. Grimmond. 2013. "High Resolution Simulation of the Variability  
39 of Surface Energy Balance Fluxes Across Central London with Urban Zones for  
40 Energy Partitioning." *Boundary-Layer Meteorology* no. 147 (3):493-523. doi:  
41 10.1007/s10546-013-9797-y.
- 42  
43  
44  
45  
46  
47  
48  
49  
50  
51  
52  
53  
54  
55  
56  
57  
58  
59  
60  
61  
62  
63  
64  
65

- 1  
2  
3  
4  
5  
6  
7  
8  
9  
10  
11  
12  
13  
14  
15  
16  
17  
18  
19  
20  
21  
22  
23  
24  
25  
26  
27  
28  
29  
30  
31  
32  
33  
34  
35  
36  
37  
38  
39  
40  
41  
42  
43  
44  
45  
46  
47  
48  
49  
50  
51  
52  
53  
54  
55  
56  
57  
58  
59  
60  
61  
62  
63  
64  
65
- Lowry, William P. 1977. "Empirical Estimation of Urban Effects on Climate: A Problem Analysis." *Journal of Applied Meteorology* no. 16 (2):129-135. doi: 10.1175/1520-0450(1977)016<0129:eeoueo>2.0.co;2.
- Lu, Jun, Chun-die Li, Yong-chuan Yang, Xin-hui Zhang, and Ming Jin. 2012. "Quantitative evaluation of urban park cool island factors in mountain city." *Journal of Central South University* no. 19 (6):1657-1662. doi: 10.1007/s11771-012-1189-9.
- McMichael, Anthony J., Rosalie E. Woodruff, and Simon Hales. 2006. "Climate change and human health: present and future risks." *The Lancet* no. 367 (9513):859-869. doi: [https://doi.org/10.1016/S0140-6736\(06\)68079-3](https://doi.org/10.1016/S0140-6736(06)68079-3).
- Mills, Gerald, J Ching, L See, B Bechtel, and M Foley. 2015. An Introduction to the WUDAPT project. In *ICUC9 - 9th International Conference on Urban Climate jointly with 12th Symposium on the Urban Environment*. Toulouse, France: The International Association for Urban Climate (IAUC) and the American Meteorological Society (AMS)
- Ng, Edward, Chao Yuan, Liang Chen, Chao Ren, and Jimmy C. H. Fung. 2011. "Improving the wind environment in high-density cities by understanding urban morphology and surface roughness: A study in Hong Kong." *Landscape and Urban Planning* no. 101 (1):59-74. doi: <http://dx.doi.org/10.1016/j.landurbplan.2011.01.004>.
- Nichol, Janet E., Wing Yee Fung, Ka-se Lam, and Man Sing Wong. 2009. "Urban heat island diagnosis using ASTER satellite images and 'in situ' air temperature." *Atmospheric Research* no. 94 (2):276-284. doi: <http://dx.doi.org/10.1016/j.atmosres.2009.06.011>.
- O'Sullivan, D., and D. Unwin. 2014. *Geographic Information Analysis*. New York: Wiley.
- Oke, T. R. 2004. Instruments and observing methods: Report No. 81: initial guidance to obtain representative meteorological observations at urban sites. In *World Meteorological Organization, WMO/TD (1250)*. Geneva: World Meteorological Organization.
- Oke, T. R. 2006. "Towards better scientific communication in urban climate." *Theoretical and Applied Climatology* no. 84 (1):179-190. doi: 10.1007/s00704-005-0153-0.
- Oke, Tim R. 1981. "Canyon geometry and the nocturnal urban heat island: comparison of scale model and field observations." *Journal of climatology* no. 1 (3):237-254.
- Peppler, A. 1929. "Das Auto als Hilfsmittel der meteorologischen Forschung." *Das Wetter* no. 46:305-308.

- 1 Peters, Jan, Martine Van Poppel, and Jan Theunis. 2012. Air quality mapping in urban  
2 environments using mobile measurements. In *Sensing a Changing World 2012*.  
3 Wageningen, The Netherlands.
- 4  
5 PlanD. 2015. *Land Utilization in Hong Kong 2014*. Hong Kong Planning Department, 15  
6 May 2015 [cited 28 Oct 2015]. Available from  
7 [http://www.pland.gov.hk/pland\\_en/info\\_serv/statistic/landu.html](http://www.pland.gov.hk/pland_en/info_serv/statistic/landu.html).  
8  
9
- 10 Quanz, Justus, Susanne Ulrich, Daniel Fenner, Achim Holtmann, and Jonas Eimermacher.  
11 2018. "Micro-Scale Variability of Air Temperature within a Local Climate Zone in  
12 Berlin, Germany, during Summer." *Climate* no. 6 (1):5.  
13  
14
- 15 Ren, Chao, Edward Yan-yung Ng, and Lutz Katzschner. 2011. "Urban climatic map studies:  
16 a review." *International Journal of Climatology* no. 31 (15):2213-2233. doi:  
17 10.1002/joc.2237.  
18  
19
- 20 Ren, Chao, Ran Wang, Meng Cai, Yong Xu, Yinsheng Zheng, and Edward Ng. 2016. The  
21 accuracy of LCZ maps generated by the world urban database and access portal tools  
22 (WUDAPT) method: A case study of Hong Kong. Paper read at 4th Int. Conf.  
23 Countermeasure Urban Heat Islands, Singapore.  
24  
25
- 26 Rizwan, Ahmed Memon, Leung Y. C. Dennis, and Chunho Liu. 2008. "A review on the  
27 generation, determination and mitigation of Urban Heat Island." *Journal of*  
28 *Environmental Sciences* no. 20 (1):120-128. doi: 10.1016/s1001-0742(08)60019-4.  
29  
30
- 31 See, L., C. Perger, M. Duerauer, S. Fritz, B. Bechtel, J. Ching, P. Alexander, G. Mills, M.  
32 Foley, M. O' Connor, I. Stewart, J. Feddema, and V. Masson. 2015. Developing a  
33 community-based worldwide urban morphology and materials database (WUDAPT)  
34 using remote sensing and crowdsourcing for improved urban climate modelling.  
35 Paper read at 2015 Joint Urban Remote Sensing Event (JURSE), March 30 2015-  
36 April 1 2015.  
37  
38
- 39 Shi, Yuan, Lutz Katzschner, and Edward Ng. 2018. "Modelling the fine-scale spatiotemporal  
40 pattern of urban heat island effect using land use regression approach in a megacity."  
41 *Science of The Total Environment* no. 618:891-904. doi:  
42 <https://doi.org/10.1016/j.scitotenv.2017.08.252>.  
43  
44
- 45 Shi, Yuan, Kevin Ka-Lun Lau, and Edward Ng. 2016. "Developing Street-Level PM2.5 and  
46 PM10 Land Use Regression Models in High-Density Hong Kong with Urban  
47 Morphological Factors." *Environmental Science & Technology* no. 50 (15):8178-8187.  
48 doi: 10.1021/acs.est.6b01807.  
49  
50  
51  
52  
53  
54  
55  
56  
57  
58  
59  
60  
61  
62  
63  
64  
65



- 1 Shi, Yuan, Chao Ren, Yingsheng Zheng, and Edward Ng. 2015. "Mapping the urban  
2 microclimatic spatial distribution in a sub-tropical high-density urban environment."  
3 *Architectural Science Review*:1-15. doi: 10.1080/00038628.2015.1105195.  
4
- 5 Siu, L. W., and M. A. Hart. 2012. "Quantifying urban heat island intensity in Hong Kong  
6 SAR, China." *Environ Monit Assess*. doi: 10.1007/s10661-012-2876-6.  
7
- 8 Skarbit, Nóra, Iain D. Stewart, János Unger, and Tamás Gál. 2017. "Employing an urban  
9 meteorological network to monitor air temperature conditions in the 'local climate  
10 zones' of Szeged, Hungary." *International Journal of Climatology* no. 37 (S1):582-  
11 596. doi: doi:10.1002/joc.5023.  
12
- 13 Stewart, I. D. 2011. "A systematic review and scientific critique of methodology in modern  
14 urban heat island literature." *International Journal of Climatology* no. 31 (2):200-217.  
15 doi: doi:10.1002/joc.2141.  
16
- 17 Stewart, I. D., and T. R. Oke. 2012. "Local Climate Zones for Urban Temperature Studies."  
18 *Bulletin of the American Meteorological Society* no. 93 (12):1879-1900. doi:  
19 10.1175/bams-d-11-00019.1.  
20
- 21 Stewart, Iain D., T. R. Oke, and E. Scott Krayenhoff. 2014. "Evaluation of the 'local climate  
22 zone' scheme using temperature observations and model simulations." *International  
23 Journal of Climatology* no. 34 (4):1062-1080. doi: doi:10.1002/joc.3746.  
24
- 25 Stewart, ID, and TR Oke. 2009. "A new classification system for urban climate sites."  
26 *Bulletin of the American Meteorological Society* no. 90 (7):922-923.  
27
- 28 Stone, Brian, Jeremy J Hess, and Howard Frumkin. 2010. "Urban form and extreme heat  
29 events: are sprawling cities more vulnerable to climate change than compact cities."  
30 *Environmental health perspectives* no. 118 (10):1425-1428.  
31
- 32 Szymanowski, M., and M. Kryza. 2009. "GIS-based techniques for urban heat island  
33 spatialization." *Climate Research* no. 38 (2):171-187.  
34
- 35 Tan, Jianguo, Youfei Zheng, Xu Tang, Changyi Guo, Liping Li, Guixiang Song, Xinrong  
36 Zhen, Dong Yuan, Adam J. Kalkstein, Furong Li, and Heng Chen. 2010. "The urban  
37 heat island and its impact on heat waves and human health in Shanghai."  
38 *International Journal of Biometeorology* no. 54 (1):75-84. doi: 10.1007/s00484-009-  
39 0256-x.  
40
- 41 Taylor, Bruce. 1986. "GEOGRAPHY IN HONG KONG." *The Professional Geographer* no.  
42 38 (4):419-423. doi: 10.1111/j.0033-0124.1986.00419.x.  
43  
44  
45  
46  
47  
48  
49  
50  
51  
52  
53  
54  
55  
56  
57  
58  
59  
60  
61  
62  
63  
64  
65

- 1  
2 Tsin, Pak Keung, Anders Knudby, E. Scott Krayenhoff, Hung Chak Ho, Michael Brauer, and  
3 Sarah B. Henderson. 2016. "Microscale mobile monitoring of urban air temperature."  
4 *Urban Climate* no. 18:58-72. doi: <https://doi.org/10.1016/j.uclim.2016.10.001>.
- 5 Unger, János, Stevan Savić, Tamás Mátyás Gál, Dragan Milošević, Enikő Lelovics, Vladimir  
6 Marković, Ágnes Gulyás, and Daniela Arsenović. 2015. Urban climate monitoring  
7 networks based on LCZ concept. In *ICUC9 - 9th International Conference on Urban*  
8 *Climate jointly with 12th Symposium on the Urban Environment*. Toulouse, France.
- 9 Unger, János, Zoltán Sümegehy, and Judit Zoboki. 2001. "Temperature cross-section features  
10 in an urban area." *Atmospheric Research* no. 58 (2):117-127. doi:  
11 [http://dx.doi.org/10.1016/S0169-8095\(01\)00087-4](http://dx.doi.org/10.1016/S0169-8095(01)00087-4).
- 12 Wang, Ran, Chao Ren, Yong Xu, Kevin Ka-Lun Lau, and Yuan Shi. 2017. "Mapping the  
13 local climate zones of urban areas by GIS-based and WUDAPT methods: A case  
14 study of Hong Kong." *Urban Climate* no. In Press. doi:  
15 <https://doi.org/10.1016/j.uclim.2017.10.001>.
- 16 WHO. 2003. Climate change and human health: risks and responses: summary. Geneva:  
17 World Health Organization. Dept. of Protection of the Human Environment.
- 18 Xu, Yong, Chao Ren, Peifeng Ma, Justin Ho, Weiwen Wang, Kevin Ka-Lun Lau, Hui Lin,  
19 and Edward Ng. 2017. "Urban morphology detection and computation for urban  
20 climate research." *Landscape and Urban Planning* no. 167 (Supplement C):212-224.  
21 doi: <https://doi.org/10.1016/j.landurbplan.2017.06.018>.
- 22 Zheng, Y., C. Ren, E. Ng, K. Lau, Y. Shi, and J.C.K. Ho. 2015. Spatial distribution of urban  
23 heat island and intra-urban air temperature variability in high-density urban areas in  
24 Hong Kong. In *9th International Conference on Urban Climate*. Toulouse, France:  
25 IAUC and AMS.
- 26 Zheng, Yingsheng, Chao Ren, Yong Xu, Ran Wang, Justin Ho, Kevin Lau, and Edward Ng.  
27 2017. "GIS-based mapping of Local Climate Zone in the high-density city of Hong  
28 Kong." *Urban Climate* no. In Press. doi: <https://doi.org/10.1016/j.uclim.2017.05.008>.
- 29  
30  
31  
32  
33  
34  
35  
36  
37  
38  
39  
40  
41  
42  
43  
44  
45  
46  
47  
48  
49  
50  
51  
52  
53  
54  
55  
56  
57  
58  
59  
60  
61  
62  
63  
64  
65

# Evaluating the Local Climate Zone Classification in High-Density Heterogeneous Urban Environment Using Mobile Measurement

Yuan SHI <sup>a,\*</sup>, Kevin Ka-Lun LAU <sup>b,c,d</sup>, Chao REN <sup>a,b,c</sup>, Edward NG <sup>a,b,c</sup>

<sup>a</sup> School of Architecture, The Chinese University of Hong Kong, Shatin, N.T., Hong Kong S.A.R., China

<sup>b</sup> The Institute of Environment, Energy and Sustainability (IEES), The Chinese University of Hong Kong, Shatin, N.T., Hong Kong S.A.R., China

<sup>c</sup> Institute Of Future Cities (IOFC), The Chinese University of Hong Kong, Shatin, N.T., Hong Kong S.A.R., China

<sup>d</sup> CUHK Jockey Club Institute of Ageing, The Chinese University of Hong Kong, Shatin, N.T., Hong Kong S.A.R., China

The corresponding author's\* email addresses: [shiyuan@cuhk.edu.hk](mailto:shiyuan@cuhk.edu.hk) (Secondary email: [shiyuan.arch.cuhk@gmail.com](mailto:shiyuan.arch.cuhk@gmail.com))

Phone: +852-39439428. Postal addresses: Rm905, YIA Building, The Chinese University of Hong Kong, Shatin, NT, Hong Kong

---

This document contains supplementary material related to the research article titled “Evaluating the Local Climate Zone Classification in High-Density Heterogeneous Urban Environment Using Mobile Measurement”. It includes three enlarged figures of the mobile measurement data which are necessary to be available to readers.

## List of Figures

Figure S - 1. The spatial variation of measured screen-level $T_a$ along the two measurement routes during the morning (09:00-11:00).....	2
Figure S - 2. The spatial variation of measured screen-level $T_a$ along the two measurement routes during the afternoon (14:00-16:00).....	2
Figure S - 3. The spatial variation of measured screen-level $T_a$ along the two measurement routes during the evening (19:00-21:00).....	3



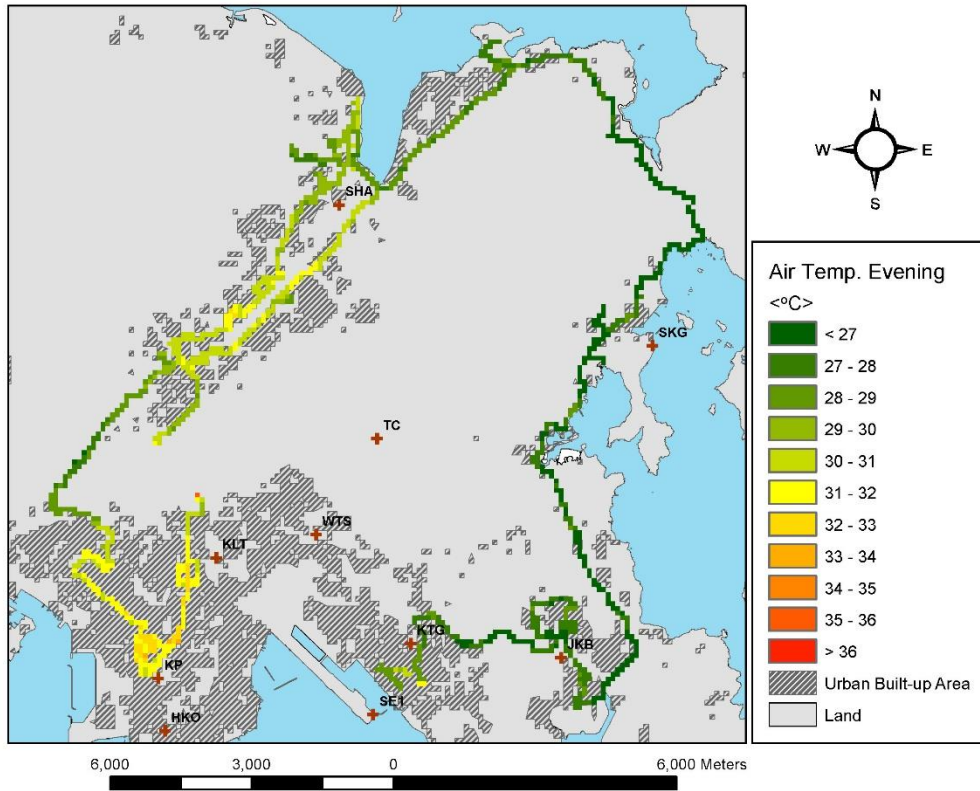


Figure S - 3. The spatial variation of measured screen-level  $T_a$  along the two measurement routes during the evening (19:00-21:00).